LETTER

https://doi.org/10.1038/s41586-018-0353-2

Accumulation of succinate controls activation of adipose tissue thermogenesis

Evanna L. Mills[1,2], Kerry A. Pierce[3], Mark P. Jedrychowski[1,2], Ryan Garrity[1], Sally Winther[1,2], Sara Vidoni[1,2], Takeshi Yoneshiro[4], Jessica B. Spinelli[2], Gina Z. Lu[1], Lawrence Kazak[5], Alexander S. Banks[6], Marcia C. Haigis[2], Shingo Kajimura[4], Michael P. Murphy[7], Steven P. Gygi[2], Clary B. Clish[3] & Edward T. Chouchani[1,2]*

Thermogenesis by brown and beige adipose tissue, which requires activation by external stimuli, can counter metabolic disease[1]. Thermogenic respiration is initiated by adipocyte lipolysis through cyclic AMP–protein kinase A signalling; this pathway has been subject to longstanding clinical investigation[2–4]. Here we apply a comparative metabolomics approach and identify an independent metabolic pathway that controls acute activation of adipose tissue thermogenesis in vivo. We show that substantial and selective accumulation of the tricarboxylic acid cycle intermediate succinate is a metabolic signature of adipose tissue thermogenesis upon activation by exposure to cold. Succinate accumulation occurs independently of adrenergic signalling, and is sufficient to elevate thermogenic respiration in brown adipocytes. Selective accumulation of succinate may be driven by a capacity of brown adipocytes to sequester elevated circulating succinate. Furthermore, brown adipose tissue thermogenesis can be initiated by systemic administration of succinate in mice. Succinate from the extracellular milieu is rapidly metabolized by brown adipocytes, and its oxidation by succinate dehydrogenase is required for activation of thermogenesis. We identify a mechanism whereby succinate dehydrogenase-mediated oxidation of succinate initiates production of reactive oxygen species, and drives thermogenic respiration, whereas inhibition of succinate dehydrogenase supresses thermogenesis. Finally, we show that pharmacological elevation of circulating succinate drives UCP1-dependent thermogenesis by brown adipose tissue in vivo, which stimulates robust protection against diet-induced obesity and improves glucose tolerance. These findings reveal an unexpected mechanism for control of thermogenesis, using succinate as a systemically-derived thermogenic molecule.

Activation of thermogenesis in brown and beige adipose tissues increases energy expenditure and can ameliorate metabolic disease[1]. Exposure to environmental cold drives adrenergic stimulation and heat production in brown adipose tissue (BAT), and improves metabolic profiles in mice[5] and humans[6]. However, pharmacological targeting of adrenergic receptors has so far demonstrated limited clinical efficacy[2–4]. Here we investigate the hypothesis that independent metabolic signals may contribute to acute activation of thermogenesis in BAT and beige fat. We applied a comparative metabolomics approach to identify metabolic signatures of thermogenesis in mouse adipose tissue (Fig. 1a), which gated on three criteria: (i) metabolite enrichment in thermogenic adipose tissue (BAT versus subcutaneous white adipose tissue; Fig. 1b); (ii) metabolite abundance in thermogenic adipose tissue (estimated as the 10% most abundant annotated metabolite ion intensities; Fig. 1c); (iii) increased metabolite abundance upon acute activation of BAT thermogenesis by exposure to 4 °C versus 29 °C (Fig. 1d). Only two metabolites fulfilled all three criteria for a thermogenic signature (Fig. 1a–d and Supplementary Tables 1–3). One of these was the mitochondrial tricarboxylic acid (TCA) cycle intermediate succinate, and the other was AMP. In 4 °C-activated BAT, succinate levels were markedly and selectively increased compared to other TCA cycle metabolites (Fig. 1 e, f and Extended Data Fig. 1a, b). Additionally, increasing beige adipocyte content in subcutaneous adipose tissue by chronic exposure to 4 °C significantly increased succinate concentration (Fig. 1g).

To investigate the role of succinate in BAT thermogenesis we explored the mechanisms responsible for driving its selective accumulation. Whereas pharmacological β-adrenergic stimulation of BAT was sufficient to drive triglyceride lipolysis (Extended Data Fig. 2a–c), stimulation of β1, β2 or β3-adrenergic receptors had no effect on succinate levels in BAT (Extended Data Fig. 2d). Therefore, selective and substantial accumulation of succinate is a signature of adipose tissue thermogenesis upon cold exposure, but not β-adrenergic signalling. Next, we tested the role of inputs to succinate from TCA metabolism by oxidation of carbons from glucose and fatty acids (Extended Data Fig. 3a). Following intravenous bolus injection, [U-^{13}C]glucose was taken up by BAT (Extended Data Fig. 3b) and oxidized by the TCA cycle (Extended Data Fig. 3c–h). Labelled $m+3$ lactate was increased in comparison to other glycolytic intermediates (Extended Data Fig. 3d). Therefore, BAT may use circulating lactate as a major carbon source for the TCA cycle in vivo, consistent with recent observations in other tissues[7,8]. However, the fractional contribution of [U-^{13}C]glucose to succinate was unchanged in BAT following exposure to 4 °C and was comparable to other TCA cycle metabolites (Extended Data Fig. 3f). [U-^{13}C]palmitate, administered by intravenous bolus, was also readily taken up by BAT (Extended Data Fig. 3i), and TCA cycle intermediates were enriched in ^{13}C derived from palmitate oxidation (Extended Data Fig. 3j–m). Following exposure to 4 °C the fractional contribution of [U-^{13}C]palmitate to succinate remained unchanged and was comparable to that in other TCA cycle metabolites (Extended Data Fig. 3k).

Apparent conventional operation of the TCA cycle (Extended Data Fig. 3b–m), concomitant with the unusual selectivity of succinate accumulation upon activation of thermogenesis (Fig. 1e, f), led us to consider whether BAT may sequester succinate from the circulation (Fig. 2a). Most mammalian cell membranes are thought to be impermeable to succinate[9,10]. However, circulating succinate levels are substantial and dynamic, and reported extracellular concentrations range from low micromolar to millimolar[11–13]. Consistent with our hypothesis, exposure of mice to 4 °C led to elevation in circulating succinate (Extended Data Fig. 4a), suggesting that this extracellular pool of succinate may contribute to accumulation in BAT. To test this idea, we monitored differentiated primary brown adipocytes incubated in standard medium, which lacks succinate. Under these conditions succinate concentrations were reduced compared to in vivo BAT (Extended Data Fig. 4b), whereas supplementation of the medium with [U-^{13}C]succinate led to substantial increase of intracellular succinate

[1]Department of Cancer Biology, Dana–Farber Cancer Institute, Boston, MA, USA. [2]Department of Cell Biology, Harvard Medical School, Boston, MA, USA. [3]Broad Institute of Harvard and MIT, Cambridge, MA, USA. [4]Diabetes Center, University of California, San Francisco, San Francisco, CA, USA. [5]Goodman Cancer Research Centre, McGill University, Montreal, Quebec, Canada. [6]Division of Endocrinology, Diabetes, and Hypertension, Brigham and Women's Hospital and Harvard Medical School, Boston, MA, USA. [7]MRC Mitochondrial Biology Unit, University of Cambridge, Cambridge Biomedical Campus, Cambridge, UK. *e-mail: edwardt_chouchani@dfci.harvard.edu

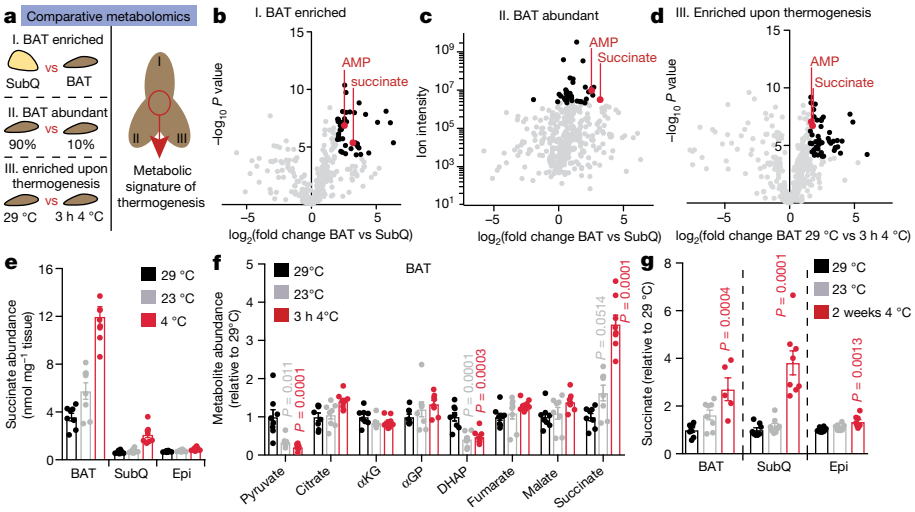

Fig. 1 | Selective accumulation of succinate is a metabolic signature of adipose tissue thermogenesis. a–d, Comparative metabolomics strategy (**a**). Grey, annotated metabolites; black, metabolites fulfilling each individual criterion; red, metabolites fulfilling all criteria. BAT-enriched metabolites (**b**) were defined as those that were enriched more than fourfold ($-\log P > 4$) in BAT versus subcutaneous inguinal adipose tissue (SubQ). Abundant BAT metabolites (**c**) were defined as those within the 10% most abundant annotated metabolite ion intensities; although determination of abundance in this way is not absolute, as ion intensity can vary between species on the basis of factors other than abundance. BAT metabolites enriched upon activation of thermogenesis by exposure to 4 °C for 3 h (**d**) were defined as those that were enriched more than threefold ($-\log P > 4$) versus BAT in mice housed at 29 °C ($n = 8$). **e**, Absolute succinate content in adipose tissues ($n = 8$). Conditions: BAT, 3 h at 4 °C; SubQ and epididymal fat (Epi) 2 weeks at 4 °C. **f**, Abundance of mitochondrial and proximal metabolites in BAT at 29 °C, 23 °C, and 3-h exposure to 4 °C ($n = 8$). αKG, α-ketoglutarate; αGP, α-glycerophosphate. **g**, Abundance of succinate in BAT, SubQ, and epididymal adipose tissue, comparing exposure at 29 °C to 2 weeks at 4 °C ($n = 8$, except 2 weeks 4 °C BAT, $n = 5$). Univariate two-sided *t*-test (**b**–**d**); one-way ANOVA (**f**, **g**); data are mean ± s.e.m. of biologically independent samples.

levels (Fig. 2b). This capacity for succinate internalization was not observed in differentiated white adipocytes or pre-adipocytes isolated from BAT (Fig. 2c). Moreover, brown adipocytes did not display comparable capacity to internalize the structurally similar mitochondrial dicarboxylates fumarate and α-ketoglutarate (Fig. 2d).

Succinate internalization by brown adipocytes resulted in accumulation of labelled $m + 4$ isotopologues of TCA cycle metabolites downstream of mitochondrial succinate oxidation (Fig. 2e and Extended Data Fig. 4c–e). Additionally, we observed mitochondrial cataplerosis and accumulation of $m + 4$ aspartate and $m + 2$ and $m + 3$ citrate

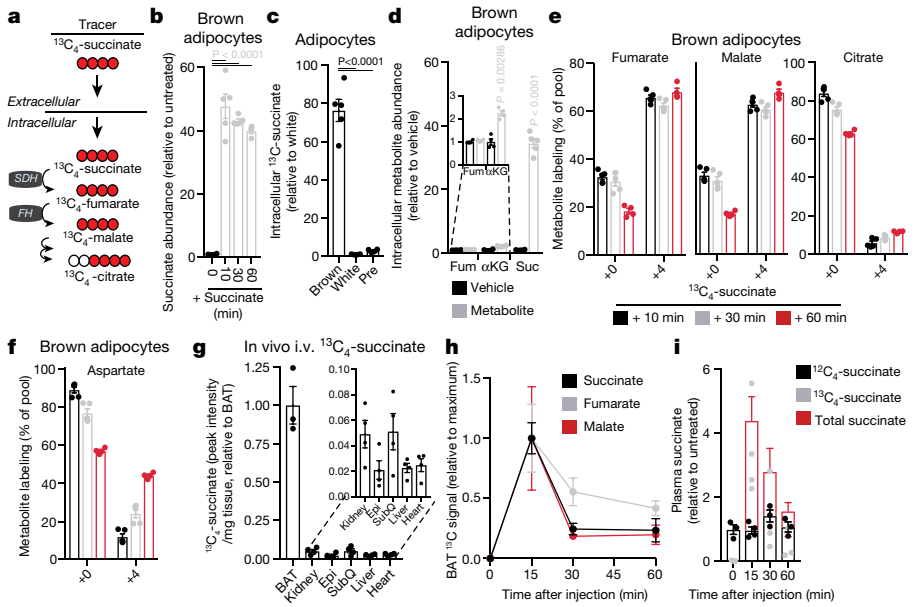

Fig. 2 | Brown adipocytes accumulate and oxidize extracellular succinate. a, Model for extracellularly driven succinate accumulation in brown adipocytes. **b**, Intracellular abundance of succinate in brown adipocytes following addition of extracellular succinate (0 min, 60 min, $n = 4$; 10 min, 30 min, $n = 5$). **c**, Abundance of intracellular ($m + 4$) [^{13}C] succinate 10 min after treatment with [^{13}C]succinate in brown ($n = 5$), white ($n = 4$), and pre-adipocytes (Pre) ($n = 4$). **d**, Intracellular abundance of TCA cycle metabolites fumarate (Fum) ($n = 4$), α-ketoglutarate (αKG) ($n = 4$) and succinate (Suc) ($n = 5$) in brown adipocytes 10 min following extracellular addition. **e**, **f**, ^{13}C-isotopologue ($m + 0$ and $m + 4$) profile of metabolites downstream of mitochondrial succinate oxidation in brown adipocytes following extracellular addition of [^{13}C]succinate ($n = 5$). **g**, Abundance of [^{13}C]succinate in mouse tissues 15 min after intravenous bolus injection of 100 mg kg^{-1} of [^{13}C]succinate ($n = 4$; except BAT, $n = 3$). **h**, Abundance of ($m + 4$) TCA cycle metabolites in BAT following intravenous bolus injection of 100 mg kg^{-1} of [^{13}C]succinate ($n = 3$). **i**, Abundance of ($m + 4$) [^{13}C]succinate and total succinate in plasma following intravenous bolus injection of 100 mg kg^{-1} of [^{13}C]succinate ($n = 3$, except 15 min, $n = 4$). One-way ANOVA (**b**, **c**); two-sided *t*-test (**d**); data are mean ± s.e.m. of biologically independent samples.

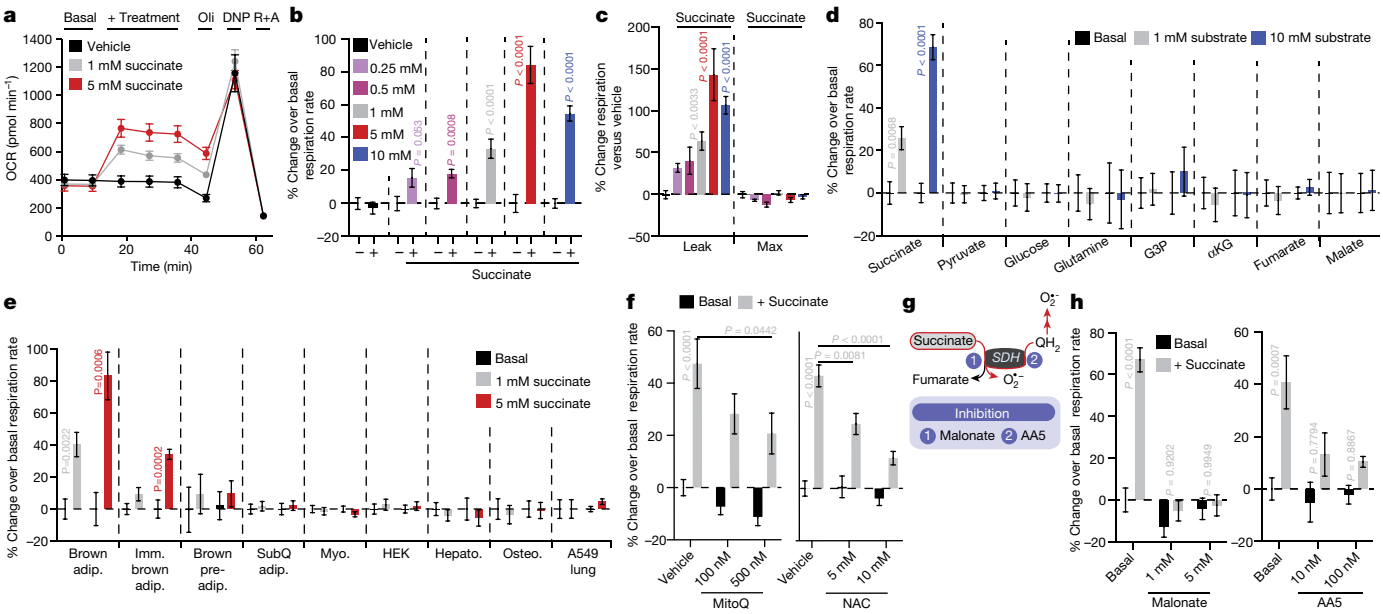

Fig. 3 | Succinate controls brown adipocyte thermogenesis via SDH oxidation and ROS production. a, Oxygen consumption rate (OCR) of brown adipocytes with or without acute succinate (vehicle, 5 mM succinate, $n = 7$; 1 mM succinate, $n = 6$). Oli, oligomycin; DNP, 2,4-dinitrophenol; R+A, rotenone/antimycin. **b**, **c**, Effect of addition of extracellular succinate on brown adipocyte OCR (**b**), leak respiration and chemically uncoupled respiration (Max) (**c**; vehicle, $n = 20$; 0.25 mM, $n = 6$; 0.5 mM, $n = 7$; 1 mM, $n = 18$; 5 mM, $n = 13$; 10 mM, $n = 12$). **d**, Effect of addition of mitochondrial and cellular substrates on brown adipocyte OCR (1 mM, $n = 6$; 10 mM, $n = 7$; 10 mM glycerol 3-phosphate (G3P), $n = 6$; 10 mM α−ketoglutarate, 10 mM fumarate, $n = 5$). **e**, Effect of acute addition of succinate on cellular OCR across different cell types. (1 mM, $n = 6$; 5 mM, $n = 7$; 5 mM brown pre-adipocyte, 5 mM SubQ adipocyte, $n = 5$). Myo, myocyte; hepato, hepatocyte; osteo, osteocyte. **f**, Inhibition of succinate-stimulated OCR by MitoQ or NAC (MitoQ vehicle, $n = 15$; 100 nM MitoQ, $n = 18$; 500 nM MitoQ, $n = 17$; NAC vehicle, $n = 7$; 5 mM NAC, $n = 6$; 10 mM NAC $n = 7$). **g**, Potential pathways of succinate-driven thermogenic ROS. **h**, Effect on succinate-stimulated OCR by inhibition of pathways linked to succinate oxidation by SDH ($n = 12$, except 5 mM malonate, $n = 11$; Atpenin A5 (AA5) vehicle, $n = 11$; 10 nM AA5, 100 nM AA5, $n = 6$). Two-sided *t*-test (**b**, **d**, **e**); one-way ANOVA (**c**); two-way ANOVA (**f**, **h**); data are mean ± s.e.m. of biologically independent samples.

(Fig. 2f and Extended Data Fig. 4e, f). [U-^{13}C]succinate administered by intravenous bolus injection was also rapidly and efficiently accumulated in BAT in vivo (Fig. 2g), coinciding with metabolism of succinate to downstream TCA cycle metabolites (Fig. 2h and Extended Data Fig. 4g) and clearance of [U-^{13}C]succinate from blood plasma (Fig. 2i and Extended Data Fig. 4h). Therefore, our results indicate that brown adipocytes have the capacity to accumulate and oxidize succinate from the extracellular milieu.

BAT accumulates increased circulating succinate (Fig. 2g), the levels of which increase upon exposure to 4 °C (Extended Data Fig. 4a). This suggests that upon exposure to cold, peripheral tissues supply succinate to BAT via the circulation. Interventions that drive muscle contraction, such as exercise, are also known to result in increased circulating succinate[11]. Since muscle shivering is an early response to exposure to environmental cold, we hypothesized that this contractile activity could drive succinate release from muscle to supply BAT accumulation. Upon exposure of mice to 4 °C for 30 min, we observed extensive shivering by electromyography (EMG) (Extended Data Fig. 4i). The shivering could be inhibited using the nicotinic acetylcholine receptor inhibitor curare (Extended Data Fig. 4i); this significantly blunted cold-dependent accumulation of succinate in BAT (Extended Data Fig. 4j). These findings suggest that shivering muscle can be a source of succinate, although effects of curare on respiratory function may also contribute.

To investigate the potential role of succinate accumulation in brown adipocyte thermogenesis, we exploited the capacity of these cells to rapidly internalize extracellular succinate (Fig. 2b). Addition of succinate to brown adipocytes resulted in acute and robust concentration-dependent stimulation of respiration (Fig. 3a, b). Succinate-stimulated respiration was specifically attributable to leak respiration, which in brown adipocytes is dependent on UCP1, and is responsible for thermogenesis in these cells[14] (Fig. 3c). Succinate utilization had no effect on chemically-uncoupled maximal respiration, indicating that its effects were not attributable to increased mitochondrial substrate supply[15] (Fig. 3c). Moreover, succinate exhibited a distinct capacity to elevate respiration when compared to other respiratory substrates (Fig. 3d and Extended Data Fig. 4k, l). By testing a panel of cell types, we found that the capacity for succinate-stimulated respiration was limited to mature primary brown adipocytes, immortalized mouse brown adipocytes, and immortalized human brown adipocytes (Fig. 3e and Extended Data Fig. 5a–e). Notably, broad pharmacological inhibition of plasma membrane transport or inhibition of plasma membrane secondary active transport via the Na^+/K^+-ATPase inhibited succinate-stimulated respiration (Extended Data Fig. 5f–k). Succinate-stimulated respiration did not require ligation of the G-protein coupled succinate receptor (SUCNR1; Extended Data Fig. 6a), elevation of cAMP levels (Extended Data Fig. 6b), activation of protein kinase A (PKA) signalling (Extended Data Fig. 6c), or elevated lipolysis (Extended Data Fig. 6d). Therefore, succinate-dependent thermogenesis is independent of SUCNR1 signalling and the lipolytic cascade.

Mitochondrial succinate oxidation can drive elevated reactive oxygen species (ROS) formation[16], which prompted us to investigate this pathway of intracellular succinate utilization. Increased ROS levels in brown adipocytes can support thermogenesis[17], but the mechanisms that control thermogenic ROS production are unknown. We found that the thermogenic effects of succinate were recapitulated in isolated BAT mitochondria (Extended Data Fig. 6e–g), and that the mitochondrial dicarboxylate carrier SLC25A10 is highly expressed in BAT (Extended Data Fig. 6h). SLC25A10 mediates rapid equilibration of mitochondrial and cytosolic succinate pools, suggesting that mitochondria in brown adipocytes can access extracellular succinate. Indeed, chemical inhibition of SLC25A10 blunted succinate-driven respiration (Extended Data Fig. 6i, j).

Furthermore, addition of succinate to brown adipocytes resulted in a rapid and robust increase in ROS levels (Extended Data Fig. 6k–m),

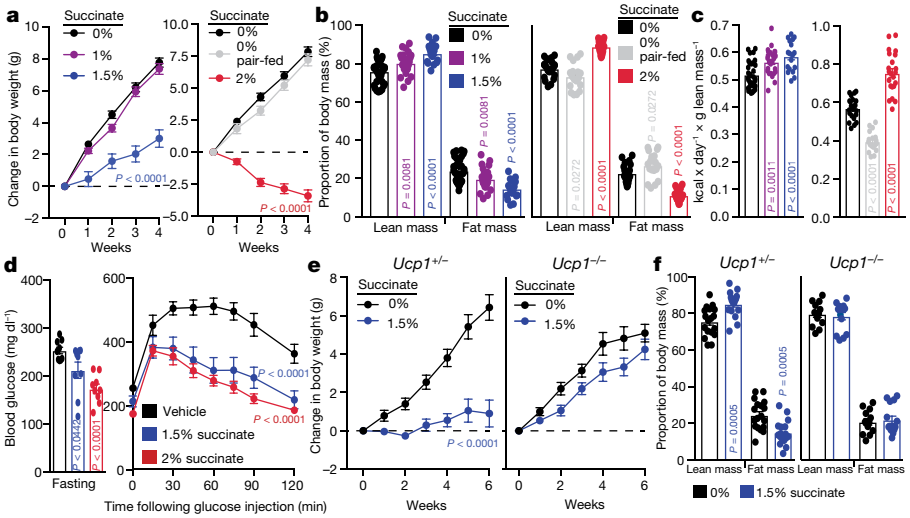

Fig. 4 | Increase of systemic succinate stimulates UCP1-dependent thermogenesis in vivo and protects against obesity. a, Body mass change during high-fat feeding with or without sodium succinate. Left: 0%, $n = 35$; 1%, $n = 26$; 1.5%, $n = 18$. Right: 0%, $n = 24$; 2%, $n = 22$; 0% pair fed, $n = 18$). **b**, Body composition of mice following 4 weeks high-fat feeding with or without low (0%, $n = 35$; 1%, $n = 26$; 1.5%, $n = 18$) or high succinate (0%, $n = 24$; 2%, $n = 22$; 0% pair fed $n = 18$). **c**, Mouse whole-body energy expenditure during 4 weeks high-fat feeding with or without low (0%, $n = 35$; 1%, $n = 26$; 1.5%, $n = 18$) or high succinate (0%, $n = 24$; 2%, $n = 22$; 0% pair fed, $n = 18$). **d**, Blood glucose parameters following 4 weeks high-fat feeding with or without succinate ($n = 9$). **e**, **f** Change in body mass (**e**) and body composition (**f**) during high-fat feeding in *Ucp1*$^{+/-}$ and *Ucp1*$^{-/-}$ mice with or without 1.5% sodium succinate (*Ucp1*$^{+/-}$ 0%, $n = 18$; *Ucp1*$^{+/-}$ 1.5%, $n = 17$; *Ucp1*$^{-/-}$ 0%, $n = 13$; UCP1(KO) 1.5%, $n = 15$). Two-way ANOVA (**a**, **d** (right), **e**); one-way ANOVA (**b**, **c**, **d** (left)); two-sided *t*-test (**f**); data are mean ± s.e.m. of biologically independent samples.

indicating that it is a potent driver of ROS in these cells. Since cysteine residues in proteins are the principal signalling targets of thermogenic ROS[17], we profiled the oxidation status of catalytic cysteines in the peroxiredoxin (Prx) family. Prx cysteines are major targets of ROS, exhibiting hyperoxidation to sulfonic acid (SO_3^-) in response to elevated ROS levels. Prx3, the only Prx isoform that is expressed exclusively in the mitochondrial matrix, exhibited increased cysteine thiol hyperoxidation to SO_3^- following succinate treatment, whereas Prx1, Prx2, Prx4 and Prx5 did not (Extended Data Fig. 7a, b and Supplementary Information). Next, we depleted either succinate-induced mitochondrial ROS using the mitochondria-targeted antioxidant MitoQ[18], or inhibited ROS-dependent cysteine oxidation using *N*-acetyl cysteine (NAC). These treatments markedly inhibited succinate-dependent respiration (Fig. 3f and Extended Data Fig. 7c). By contrast, increasing the cysteine oxidation state with diamide was sufficient to drive respiration in brown adipocytes (Extended Data Fig. 7d, e).

Succinate could control ROS levels by fuelling superoxide production through a number of electron circuits in the mitochondrial respiratory chain (Fig. 3g and Extended Data Fig. 7f). All of these pathways require succinate oxidation by the flavin site on succinate dehydrogenase (SDH) (Fig. 3g). Treatment of brown adipocytes with malonate, a competitive inhibitor of succinate oxidation by the SDH flavin[19] (Fig. 3g and Extended Data Fig. 7f), abrogated both succinate-dependent ROS production and succinate-dependent respiration (Fig. 3h and Extended Data Fig. 7g–i). We then systematically manipulated the downstream superoxide-producing sites linked to succinate oxidation (Extended Data Fig. 7f). Inhibition at the SDH Q-site[20] fully inhibited succinate-dependent respiration (Fig. 3h and Extended Data Fig. 7j), indicating that electron transfer between SDH and ubiquinone was required. Conversely, inhibitors of ROS production through mitochondrial complex I[21], mitochondrial complex III[22], or α-glycerophosphate dehydrogenase[23] (αGPDH) did not have as substantial effects on succinate-stimulated respiration (Extended Data Fig. 7k–q), but these sites may be relevant and will be more fully explored in future studies.

Our findings suggest a model for an activation pathway of adipocyte thermogenic respiration: BAT possesses the capacity to utilize high levels of extracellular succinate (Fig. 2), and can rapidly oxidize succinate via SDH to drive mitochondrial Q-pool reduction, ROS production and thermogenesis (Fig. 3). This model predicts that acute increase of systemic succinate should be sufficient to drive BAT thermogenesis in vivo. We found that intravenous injection of succinate resulted in a rapid increase in interscapular BAT temperature (Extended Data Fig. 8a) and whole-body oxygen consumption (Extended Data Fig. 8b). These effects peaked at the time of maximal accumulation of circulating succinate in BAT (Fig. 2h). Since these experiments were performed in conscious free-moving mice there was a substantial effect of handling stress that, when accounted for, revealed succinate-dependent effects[24] (Extended Data Fig. 8b). Notably, in mice lacking UCP1 (UCP1(KO)) the thermogenic effect of succinate was not observed (Extended Data Fig. 8b). Conversely, thermogenesis initiated by cold exposure was supressed by co-administration of the SDH inhibitor malonate (Extended Data Fig. 8c).

The effect of elevating circulating succinate resulting in UCP1-dependent thermogenesis in vivo prompted us to investigate the role of this pathway in modulation of whole-body energy expenditure in diet-induced obesity. Dietary succinate is well tolerated[25]. Moreover, we confirmed that acute oral administration resulted in increased circulating succinate[26] (Extended Data Fig. 8d). On this basis, ad libitum high-fat-diet-fed mice were provided drinking water supplemented with sodium succinate. The mice showed no aversion to succinate (Extended Data Fig. 8e, f), and exhibited a robust concentration-dependent suppression and reversal of weight gain induced by high-fat feeding over four weeks (Fig. 4a and Extended Data Fig. 8g, h) as a result of decreased fat mass (Fig. 4b). Several lines of evidence suggest that this effect was at least partly attributable to an increase in energy expenditure. First, succinate administration did not substantially inhibit ad libitum caloric intake (Extended Data Fig. 8i,j), and controlled pair-feeding recapitulated the metabolic phenotype observed under ad libitum conditions (Fig. 4b and Extended Data Fig. 8h). Furthermore, succinate supplementation did not inhibit caloric absorption or energy assimilation (Extended Data Fig. 8k, l). Most importantly, we applied the energy balance method[27,28], which indicated that succinate supplementation drove a robust increase in whole-body energy expenditure over the four-week period (Fig. 4c). These systemic effects of dietary succinate resulted in brown, subcutaneous and epididymal adipose depots exhibiting smaller adipocyte size and reduced lipid accumulation (Extended Data Fig. 9a). Additionally, livers of mice receiving dietary succinate exhibited reduced lipid

deposition, whereas heart and kidneys were morphologically indistinguishable from controls (Extended Data Fig. 9b–f).

Succinate supplementation also lowered fasting circulating glucose levels (Fig. 4d) and protected against glucose intolerance induced by high-fat feeding (Fig. 4d and Extended Data Fig. 9g). Moreover, there was no evidence of increased inflammatory or anti-inflammatory markers in adipose tissues; and in some cases, such as for interleukin-1β, there was a decrease in expression (Extended Data Fig. 9h, i). These findings are noteworthy, since in certain physiological settings, circulating succinate can engage immune cell recruitment and activation[29,30]. The lack of immunogenic signalling by succinate here could be explained by the function of thermogenic adipose tissue as a sink for succinate (Fig. 2g), rapidly clearing circulating succinate (Fig. 2h, i) that would otherwise be predicted to antagonize immunogenic signalling[29,30]. This interpretation is supported by the observation that dietary succinate potentiated inflammatory signalling in adipose depots of UCP1(KO) mice but not those of wild-type mice (Extended Data Fig. 9h), suggesting that competent thermogenic adipose tissue antagonizes inflammatory signalling by succinate in a dominant fashion. Finally, to determine whether the robust weight loss and energy expenditure effects of dietary succinate required adipose tissue thermogenesis, we examined the physiological effect of succinate supplementation in UCP1(KO) mice, a genetic model lacking thermogenically competent adipose tissue[31]. The inhibitory effects of succinate supplementation on weight gain (Fig. 4e, f and Extended Data Fig. 10a–e) and stimulatory effects on energy expenditure (Extended Data Fig. 10f) of succinate supplementation did not occur in UCP1(KO) mice.

In conclusion, we have identified a mechanism for activation of BAT thermogenesis through utilization of a systemic pool of the TCA cycle intermediate succinate. Succinate exerts acute control over adipose-tissue thermogenesis by triggering mitochondrial ROS production via SDH oxidation, and may be systemically integrated by the capacity of brown adipocytes to metabolize extracellular succinate. Therefore, as well as identifying a molecular pathway for activation of adipocyte thermogenesis, our results demonstrate that succinate acts as a previously unappreciated systemic redox signal, and exerts profound effects on whole-body metabolism.

Online content

Any Methods, including any statements of data availability and Nature Research reporting summaries, along with any additional references and Source Data files, are available in the online version of the paper at https://doi.org/10.1038/s41586-018-0353-2.

Received: 6 November 2017; Accepted: 12 June 2018;
Published online 18 July 2018.

1. Pfeifer, A. & Hoffmann, L. S. Brown, beige, and white: the new color code of fat and its pharmacological implications. *Annu. Rev. Pharmacol. Toxicol.* **55**, 207–227 (2015).
2. Cypess, A. M. et al. Cold but not sympathomimetics activates human brown adipose tissue in vivo. *Proc. Natl Acad. Sci. USA* **109**, 10001–10005 (2012).
3. Cypess, A. M. et al. Activation of human brown adipose tissue by a β3-adrenergic receptor agonist. *Cell Metab.* **21**, 33–38 (2015).
4. Carey, A. L. et al. Ephedrine activates brown adipose tissue in lean but not obese humans. *Diabetologia* **56**, 147–155 (2013).
5. Ravussin, Y., Xiao, C., Gavrilova, O. & Reitman, M. L. Effect of intermittent cold exposure on brown fat activation, obesity, and energy homeostasis in mice. *PLoS One* **9**, e85876 (2014).
6. Hanssen, M. J. et al. Short-term cold acclimation improves insulin sensitivity in patients with type 2 diabetes mellitus. *Nat. Med.* **21**, 863–865 (2015).
7. Hui, S. et al. Glucose feeds the TCA cycle via circulating lactate. *Nature* **551**, 115–118 (2017).
8. Faubert, B., et al. Lactate metabolism in human lung tumors. *Cell* **171**, 358–371 (2017).
9. Hems, R., Stubbs, M. & Krebs, H. A. Restricted permeability of rat liver for glutamate and succinate. *Biochem. J.* **107**, 807–815 (1968).
10. Ehinger, J. K. et al. Cell-permeable succinate prodrugs bypass mitochondrial complex I deficiency. *Nat. Commun.* **7**, 12317 (2016).
11. Hochachka, P. W. & Dressendorfer, R. H. Succinate accumulation in man during exercise. *Eur. J. Appl. Physiol. Occup. Physiol.* **35**, 235–242 (1976).
12. Sadagopan, N. et al. Circulating succinate is elevated in rodent models of hypertension and metabolic disease. *Am. J. Hypertens.* **20**, 1209–1215 (2007).
13. Correa, P. R. et al. Succinate is a paracrine signal for liver damage. *J. Hepatol.* **47**, 262–269 (2007).
14. Chouchani, E. T. *et al.* Mitochondrial ROS regulate thermogenic energy expenditure and sulfenylation of UCP1. *Nature* **532**, 112–116 (2016).
15. Brand, M. D. & Nicholls, D. G. Assessing mitochondrial dysfunction in cells. *Biochem. J.* **435**, 297–312 (2011).
16. Murphy, M. P. How mitochondria produce reactive oxygen species. *Biochem. J.* **417**, 1–13 (2009).
17. Chouchani, E. T., Kazak, L. & Spiegelman, B. M. Mitochondrial reactive oxygen species and adipose tissue thermogenesis: Bridging physiology and mechanisms. *J. Biol. Chem.* **292**, 16810–16816 (2017).
18. Smith, R. A. & Murphy, M. P. Animal and human studies with the mitochondria-targeted antioxidant MitoQ. *Ann. NY Acad. Sci.* **1201**, 96–103 (2010).
19. Quastel, J. H. & Wooldridge, W. R. Some properties of the dehydrogenating enzymes of bacteria. *Biochem. J.* **22**, 689–702 (1928).
20. Miyadera, H. et al. Atpenins, potent and specific inhibitors of mitochondrial complex II (succinate-ubiquinone oxidoreductase). *Proc. Natl Acad. Sci. USA* **100**, 473–477 (2003).
21. Brand, M. D. et al. Suppressors of superoxide-H_2O_2 production at site I_Q of mitochondrial complex I protect against stem cell hyperplasia and ischemia-reperfusion injury. *Cell Metab.* **24**, 582–592 (2016).
22. Orr, A. L. et al. Suppressors of superoxide production from mitochondrial complex III. *Nat. Chem. Biol.* **11**, 834–836 (2015).
23. Orr, A. L. et al. Novel inhibitors of mitochondrial *sn*-glycerol 3-phosphate dehydrogenase. *PLoS One* **9**, e89938 (2014).
24. Golozoubova, V., Cannon, B. & Nedergaard, J. UCP1 is essential for adaptive adrenergic nonshivering thermogenesis. *Am. J. Physiol. Endocrinol. Metab.* **291**, E350–E357 (2006).
25. Maekawa, A. et al. Lack of toxicity/carcinogenicity of monosodium succinate in F344 rats. *Food Chem. Toxicol.* **28**, 235–241 (1990).
26. Browne, J. L., Sanford, P. A. & Smyth, D. H. Transfer and metabolism of citrate, succinate, α-ketoglutarate and pyruvate by hamster small intestine. *Proc. R. Soc. Lond. B Biol. Sci.* **200**, 117–135 (1978).
27. Ravussin, Y., Gutman, R., LeDuc, C. A. & Leibel, R. L. Estimating energy expenditure in mice using an energy balance technique. *Int. J. Obes.* **37**, 399–403 (2013).
28. Goldgof, M. et al. The chemical uncoupler 2,4-dinitrophenol (DNP) protects against diet-induced obesity and improves energy homeostasis in mice at thermoneutrality. *J. Biol. Chem.* **289**, 19341–19350 (2014).
29. Peruzzotti-Jametti, L., et al. Macrophage-derived extracellular succinate licenses neural stem cells to suppress chronic neuroinflammation. *Cell Stem Cell* **22**, 355–368 (2018).
30. Littlewood-Evans, A. et al. GPR91 senses extracellular succinate released from inflammatory macrophages and exacerbates rheumatoid arthritis. *J. Exp. Med.* **213**, 1655–1662 (2016).
31. Kazak, L. et al. UCP1 deficiency causes brown fat respiratory chain depletion and sensitizes mitochondria to calcium overload-induced dysfunction. *Proc. Nat. Acad. Sci.* **114**, 7981–7986 (2017).

Acknowledgements This work is supported by the Claudia Adams Barr Program (E.T.C.), EMBO (E.L.M.), Novo Nordisk Foundation NFF18OC0032380 (S.W.), CIHR (L.K.), NIH-DK103295 (M.C.H), NIH-DK97441 and DK112268 (S.K.), MRC-MC_U105663142, Wellcome Trust 110159/Z/15/Z (M.P.M.), and NIH-GM067945 (S.P.G.). We thank B. Spiegelman for discussions, R. Goncalves for assistance with reagents, the Nikon Imaging Center at Harvard Medical School for assistance with microscopy, and Dana-Farber/Harvard Cancer Center (NIH-5-P30-CA06516) for preparing histology slides.

Reviewer information *Nature* thanks N. Chandel, J. Rabinowitz and the other anonymous reviewer(s) for their contribution to the peer review of this work.

Author contributions E.L.M. designed research, carried out experiments, and analysed data. K.A.P., M.P.J. and J.B.S. carried out and analysed data from mass spectrometry experiments. R.G., S.W., S.V., T.Y. and G.Z.L. carried out cellular experiments. L.K. assisted with design of in vivo experiments. A.S.B. and S.K. oversaw calorimetry and cell experiments. M.P.M. provided advice and reagents. M.C.H., S.P.G. and C.B.C. oversaw mass spectrometry experiments. E.T.C. directed research and co-wrote the paper with assistance from the other authors.

Competing interests E.T.C. and E.L.M. have applied for a patent on the basis of some of the work described here.

Additional information
Extended data is available for this paper at https://doi.org/10.1038/s41586-018-0353-2.
Supplementary information is available for this paper at https://doi.org/10.1038/s41586-018-0353-2.
Reprints and permissions information is available at http://www.nature.com/reprints.
Correspondence and requests for materials should be addressed to E.T.C.
Publisher's note: Springer Nature remains neutral with regard to jurisdictional claims in published maps and institutional affiliations.

METHODS

Animal procedures and ethics statement. Animal experiments were performed according to procedures approved by the Institutional Animal Care and Use Committee of the Beth Israel Deaconess Medical Center. Unless otherwise stated, mice used were male C57BL/6J (8–12 weeks of age; Jackson Laboratories), and housed in a temperature-controlled (23 °C) room on a 12-h light–dark cycle. Both male and female UCP1(KO) (B6.129-Ucp1tm1Kz/J) and littermate matched heterozygotes were used.

Body temperature and cold exposure. Interscapular body temperature was assessed using implantable electronic ID transponders (Bio Medic Data Systems, Inc.). When studying acute activation of thermogenesis, mice were housed from birth at 23 °C to allow for recruitment of thermogenic adipose tissue[33]. Before individual housing at 4 °C or any experiments involving acute activation of thermogenesis, mice were placed at thermoneutrality (29 °C) for 1 day, which allows both for maintenance of BAT UCP1 protein content[34] and for measurement of induction of BAT thermogenesis by acute intervention.

Metabolite analyses by mass spectrometry. Metabolites were profiled using an LC–MS system comprised of a Nexera X2 U-HPLC (Shimadzu Scientific Instruments; Marlborough, MA) coupled to a Q Exactive Plus orbitrap mass spectrometer (Thermo Fisher Scientific; Waltham, MA). Tissues were rapidly isolated and homogenized in extraction solution of 80% methanol containing inosine-$^{15}N_4$, thymine-d_4 and glycocholate-d_4 internal standards (Cambridge Isotope Laboratories; Andover, MA) at a 4:1 volume to wet weight ratio. The samples were centrifuged (10 min, 9,000*g*, 4 °C) and the supernatants were injected directly onto a 150 × 2.0 mm Luna NH2 column (Phenomenex; Torrance, CA). For analysis of TCA cycle metabolites in BAT, an additional 100× dilution was performed in extraction solution to render succinate abundance within the linear quantification range of the instrument, as described in Extended Data Fig. 1. The column was eluted at a flow rate of 400 µl/min with initial conditions of 10% mobile phase A (20 mM ammonium acetate and 20 mM ammonium hydroxide in water) and 90% mobile phase B (10 mM ammonium hydroxide in 75:25 v/v acetonitrile/methanol) followed by a 10 min linear gradient to 100% mobile phase A. Mass spectrometry analyses were carried out using electrospray ionization in the negative ion mode using full scan analysis over *m/z* 70–750 at 70,000 resolution and 3 Hz data acquisition rate. Additional mass spectrometry settings were: ion spray voltage, −3.0 kV; capillary temperature, 350 °C; probe heater temperature, 325 °C; sheath gas, 55; auxiliary gas, 10; and S-lens RF level 50. Raw data were processed using Progenesis QI software version 1.0 (NonLinear Dynamics) for feature alignment, nontargeted signal detection, and signal integration. Targeted processing of a subset of known metabolites and isotopologues was conducted using TraceFinder software version 4.1 (Thermo Fisher Scientific). Compound identities were confirmed using reference standards. Succinate was quantified using a targeted LC–MS method operated on a ACQUITY UPLC (Waters) coupled to a 5500 QTRAP mass spectrometer (SCIEX) as described previously[14,35]. For succinate analysis of mouse serum for shivering and curare experiments samples were analysed using reverse phase ion-pairing chromatography coupled to tandem mass spectrometry (Agilent LC–MS). Analytes were eluted in buffer A (97% H2O, 3% MeOH, 10 mM tributylamine, 15 mM glacial acetic acid, pH 5.5) and buffer B (10 mM tributylamine, 15 mM glacial acetic acid in 100% MeOH). Samples were run on a ZORBAX Extend-C18, 2.1 × 150 mm, 1.8 µm (Agilent) with a flow rate of 0.25 ml/min for 2.5 min of buffer A, followed by a linear gradient (100% buffer A to 80% buffer A) for 5 min, followed by a linear gradient (80% buffer A to 55% buffer A) for 5.5 min, followed by a linear gradient (55% buffer A to 1% buffer A) for 7 min, followed by 4 min with (1% buffer A). Samples were ionized using Agilent Jet Spray ionization; nebulizer 45 psi, capillary −2000 V, nozzle voltage: 500 V, sheath gas temperature 325 °C, and sheath gas flow 12 l/min. An Agilent 6470 Triple Quadrupole mass spectrometer was used for mass detection with a targeted method. Peaks were integrated in Mass Hunter (Agilent).

^{13}C metabolite tracing. [U-^{13}C]glucose (2.4 g/kg), [U-^{13}C]palmitate (80 mg/kg) or [U-^{13}C]succinate (100 mg/kg) (all from Cambridge Isotope Laboratories) were administered by tail vein injection and mice were individually housed at 4 °C or 29 °C for the indicated times before tissue harvest. [U-^{13}C]palmitate was conjugated to 1% BSA before injection. All injections were performed as a bolus over 20 s. For in vitro studies [U-^{13}C]succinate was added to BAT cells for the indicated times at a final concentration of 5 mM. Cells were washed and lysed directly in metabolite extraction buffer, snap frozen in liquid nitrogen and stored at −80 °C until MS analysis was performed.

Primary brown adipocyte preparation and differentiation. Interscapular brown adipose stromal vascular fraction was obtained from 2-to-6-day-old pups as described previously[36]. Interscapular brown adipose tissue was dissected, washed in PBS, minced, and digested for 45 min at 37 °C in PBS containing 1.5 mg ml^{-1} collagenase B, 123 mM NaCl, 5 mM KCl, 1.3 mM $CaCl_2$, 5 mM glucose, 100 mM HEPES, and 4% essentially fatty-acid-free BSA. Tissue suspension was filtered through a 40-µm cell strainer and centrifuged at 600*g* for 5 min to pellet the SVF. The cell pellet was resuspended in adipocyte culture medium and plated. Cells were maintained at 37 °C in 10% CO_2. Primary brown pre-adipocytes were counted and plated in the evening, 12 h before differentiation at 15,000 cells per well of a Seahorse plate. Pre-adipocyte plating was scaled according to surface area. The following morning, brown pre-adipocytes were induced to differentiate for 2 days with an adipogenic cocktail (1 µM rosiglitazone, 0.5 mM IBMX, 5 µM dexamethasone, 0.114 µg ml^{-1} insulin, 1 nM T3, and 125 µM indomethacin) in adipocyte culture medium. Two days after induction, cells were re-fed every 48 h with adipocyte culture medium containing 1 µM rosiglitazone, 1 nM T3, and 0.5 µg ml^{-1} insulin. Cells were fully differentiated by day 7 after induction.

Primary white adipocyte preparation and differentiation. Inguinal white adipose stromal vascular fraction was obtained from 2-to-6-day-old pups as described previously[37]. Adipose tissue was dissected, washed in PBS, minced, and digested for 45 min at 37 °C in HBSS containing collagenase D (10 mg/ml), dispase II (3 U/ml) and $CaCl_2$ (10 mM). Tissue suspension was filtered through a 40-µm cell strainer and centrifuged at 600*g* for 5 min to pellet the SVF. The cell pellet was resuspended in adipocyte culture medium supplemented with 10% fetal bovine serum (FBS) and 1% penicillin/streptomycin (P/S) and plated. Cells were maintained at 37 °C in 10% CO_2. Primary white pre-adipocytes were counted and plated in the evening, 12 h before differentiation at 15,000 cells per well of a seahorse plate. Pre-adipocyte plating was scaled according to surface area. The following morning, white pre-adipocytes were induced to differentiate for 2 days with an adipogenic cocktail (rosiglitazone (1 µM), IBMX (0.5 mM), dexamethasone (1 µM), insulin (5 µg/ml)) in adipocyte culture medium. Two days after induction, cells were re-fed every 48 h with adipocyte culture medium containing rosiglitazone (1 µM) and insulin (5 µg/ml). Cells were fully differentiated by day 6 after induction.

Immortalized human brown pre-adipocyte line differentiation. Immortalized human brown preadipocytes[38] were cultured with animal component-free medium (Stem Cell Technologies; #05449). Brown adipocyte differentiation was induced by treating confluent preadipocytes with animal component-free adipogenic differentiation medium (Stem Cell Technologies; #05412) supplemented with T3 (1 nM) and rosiglitazone (0.5 µM). Cells were fully differentiated 2 weeks after induction.

Maintenance of cell lines. All cell lines were grown in DMEM supplemented with 10% FBS and 1% P/S. Cells were detached using 0.05% trypsin and subcultured every other day.

Cellular respirometry of primary adipocytes. Cellular OCR of primary brown or white adipocytes was determined using a Seahorse XF24 Extracellular Flux Analyzer. Adipocytes were plated and differentiated in XF24 V7 cell culture microplates. Prior to analysis adipocyte culture medium was changed to respiration medium consisting of DMEM lacking $NaHCO_3$ (Sigma), NaCl (1.85 g/l), phenol red (3 mg/l), 2% fatty-acid-free BSA, and sodium pyruvate (1 mM), pH 7.4. In all cases, basal respiration was determined to be the OCR in the presence of substrate (1 mM sodium pyruvate) alone. Respiration uncoupled from ATP synthesis was determined following addition of oligomycin (4.16 µM). Maximal respiration was determined following addition of DNP (2 mM). Rotenone (3 µM) and antimycin (3 µM) were used to abolish mitochondrial respiration. Leak respiration was calculated as OCR following rotenone/antimycin treatment subtracted from OCR following oligomycin treatment.

Cellular respirometry of cell lines. Cellular OCR of cells lines was determined using a Seahorse XF24 Extracellular Flux Analyzer as described above with a few minor changes. All cell lines, except DE cells and immortalized human brown adipocytes, were plated at a density of 50,000 cells/well and a final concentration of 0.2% fatty-acid-free BSA was used. De2.3 cells and immortalized human brown adipocytes were plated at 5,000 cells/well and 30,000 cells/well, respectively, and a final concentration of 2% fatty-acid-free BSA was used. Respiration uncoupled from ATP synthesis was determined following addition of oligomycin (1.25 µM). Rotenone (3 µM) and antimycin (3 µM) were used to abolish mitochondrial respiration.

Imaging of brown adipocytes. ROS production was estimated by oxidation of DHE and ratiometric assessment. Cells were grown on 35-mm glass bottom No. 1.5 coverslips (MatTek). Ten minutes before imaging, cells were loaded with dihydroethidium (DHE, 5 µM, Sigma) in imaging buffer (NaCl, 156 mM; KCl, 3 mM; $MgCl_2$ 2 mM; KH_2PO_4, 1.25 mM; HEPES, 10 mM; sodium pyruvate, 1 mM). Cell culture dishes were mounted in a Tokai Hit INU microscope stage top incubator (37 °C and 5% CO_2). Oxidised DHE was excited at 500 nm and the emitted signal was acquired at 632 nm. Reduced DHE was excited at 380 nm and the emitted signal was acquired at 460 nm. A time-lapse was performed in which cells were imaged every 20 s using an exposure time of 30 ms, 4 × 4 camera binning and the ND4 filter in. Four images were acquired before acute treatment with compounds of interest and imaged for 10 min. All images were collected with an Inverted Nikon Ti fluorescence microscope equipped with 10× SF objective lens using MetaMorph 7.2 acquisition software and the Perfect Focus System for maintenance of focus over time. All measured cell parameters were analysed with Fiji image processing software. In brief, 5 cells were selected from each image acquired with

10× objective, background removal was performed and a ratio of oxidized DHE over reduced DHE was calculated. For high resolution images a 40× SF objective lens with a layer of mineral oil on top of the media was used and cells were imaged at one time-point, 10 min post-treatment. Images were processed using the Fiji ratio plus plugin with background correction for each channels and multiplication factors set to 1. The fluorescence images are displayed using the same setting and were pseudocolored using the fire LUT. The transmitted light images are displayed using the autoscale LUT grey scale.

Assessment of protein thiol sulfonic acids. Samples were homogenized in 50 mM Tris base, containing 100 mM NaCl, 100 μM DTPA, 0.1% SDS, 0.5% sodium deoxycholate, 0.5% Triton-X 100, 10 mM TCEP and 50 mM iodoacetamide. Following incubation for 15 min, SDS was added to a final concentration of 1% and samples were incubated for a further 15 min.

Protein digestion. Protein pellets were dried and resuspended in 8 M urea containing 50 mM HEPES (pH 8.5). Protein concentrations were measured by BCA assay (Thermo Scientific) before protease digestion. Protein lysates were diluted to 4 M urea and digested with LysC (Wako, Japan) in a 1/100 enzyme/protein ratio overnight. Protein extracts were diluted further to a 1.0 M urea concentration, and trypsin (Promega) was added to a final 1/200 enzyme/protein ratio for 6 h at 37 °C. Digests were acidified with 20 μl of 20% formic acid (FA) to a pH ~2, and subjected to C18 solid-phase extraction (50 mg Sep-Pak, Waters).

LC–MS/MS parameters for targeted Prx cysteine peptide analysis. All spectra were acquired using an Orbitrap Fusion mass spectrometer (Thermo Fisher) in line with an Easy-nLC 1000 (Thermo Fisher Scientific) ultra-high pressure liquid chromatography pump. Peptides were separated onto a 100-μM inner diameter column containing 1 cm of Magic C4 resin (5 μm, 100 Å, MichromBioresources) followed by 30 cm of SepaxTechnologies GP-C18 resin (1.8 μm, 120 Å) with a gradient consisting of 9–30% (ACN, 0.125% FA) over 180 min at ~250 nl min^{-1}. For all LC–MS/MS experiments, the mass spectrometer was operated in the data-dependent mode. We collected MS1 spectra at a resolution of 120,000, with an AGC target of 150,000 and a maximum injection time of 100 ms. The ten most intense ions were selected for MS2 (excluding 1 *Z*-ions). MS1 precursor ions were excluded using a dynamic window (75 s ± 10 ppm). The MS2 precursors were isolated with a quadrupole mass filter set to a width of 0.5 Th. For the MS3 based TMT quantitation, MS2 spectra were collected at an AGC of 4,000, maximum injection time of 200 ms, and CID collision energy of 35%. MS3 spectra were acquired with the same Orbitrap parameters as the MS2 method except HCD collision energy was increased to 55%. Synchronous- precursor-selection was enabled to include up to six MS2 fragment ions for the MS3 spectrum.

Data processing and MS2 spectra assignment. A compilation of in-house software was used to convert .raw files to mzXML format, as well as to adjust monoisotopic *m*/*z* measurements and erroneous peptide charge state assignments. Assignment of MS2 spectra was performed using the SEQUEST algorithm[39]. All experiments used the Mouse UniProt database (downloaded 10 April 2014) where reversed protein sequences and known contaminants such as human keratins were appended. SEQUEST searches were performed using a 20 ppm precursor ion tolerance, while requiring each peptide's amino/carboxy (N/C) terminus to have trypsin protease specificity and allowing up to two missed cleavages. For targeted assessment of Prx cysteine thiol sulfonic acids, TMT tags on lysine residues and peptide N termini (+229.16293 Da), iodoacetamide on cysteine residues (+57.0214637 Da) were set as static modifications and oxidation of methionine residues (+15.99492 Da) and sulfonic acid formation on cysteine residues (+9.036719 Da versus iodoacetamide) as variable modifications. Determination of sulfonic acid formation of the Prx peptides was determined by comparing TMT reporter ion abundance of sulfonic acid containing peptides normalized to the unmodified (iodoacetamide-labelled) forms. An MS2 spectra assignment false discovery rate of less than 1% was achieved by applying the target-decoy database search strategy[40]. Protein filtering was performed using an in-house linear discrimination analysis algorithm to create one combined filter parameter from the following peptide ion and MS2 spectra metrics: XCorr, ΔCn score, peptide ion mass accuracy, peptide length and missed-cleavages[41]. Linear discrimination scores were used to assign probabilities to each MS2 spectrum for being assigned correctly, and these probabilities were further used to filter the dataset to a 1% protein-level false discovery rate.

Western Blotting. Samples were isolated in 50 mM Tris, pH 7.4, 500 mM NaCl, 1% NP40, 20% glycerol, 5 mM EDTA and 1 mM phenylmethylsulphonyl fluoride, supplemented with a cocktail of protease inhibitors (Roche). Homogenates were centrifuged at 16,000*g* for 10 min at 4 °C, and the supernatants were used for subsequent analyses. Protein concentration was determined using the bicinchoninic acid assay (Pierce). Protein lysates were denatured in Laemmli buffer (60 mM Tris, pH 6.8, 2% SDS, 10% glycerol, 0.05% bromophenol blue, 100 mM DTT), resolved by 4–12% NuPAGE Bis-Tris SDS–PAGE (Invitrogen) and transferred to a polyvinylidene difluoride (PVDF) membrane. Primary antibodies (pPKA substrate (CST 9624 s); Tubulin (Abcam AB44928)) were diluted in TBS containing 0.05% Tween (TBS-T), 5% BSA and 0.02% NaN_3[41]. Membranes were incubated overnight with primary antibodies at 4 °C. For secondary antibody incubation, anti-rabbit HRP (Promega) was diluted in TBS-T containing 5% milk. Results were visualized with enhanced chemiluminescence (ECL) western blotting substrates (Pierce).

Glycerol release. Adipocytes were incubated in respiration medium and treated as indicated before collection of medium and quantification of glycerol using free glycerol reagent (Sigma-Aldrich) relative to glycerol standard.

Metabolic phenotyping. Whole-body energy metabolism was evaluated using a Comprehensive Laboratory Animal Monitoring System (CLAMS, Columbia Instruments). Mice were acclimated in the metabolic chambers and acclimated with mock injection procedures to minimize contribution of stress to the metabolic phenotype. O_2 levels were collected every 60 s. Basal O_2 consumption rate was determined to be the mean of the lowest three readings determined before intervention. Maximum O_2 consumption rate was determined as the mean of three highest rates recorded post-intervention.

Determination of free-living whole-body total energy expenditure. Whole-body energy expenditure in mice was determined using the energy balance method, otherwise known as the law of energy conservation, which accounts for caloric intake, change in body weight, and change in lean and fat mass throughout dietary intervention, as described previously[27,28,42]. Briefly, individual mouse body weight and body composition were determined before dietary intervention with or without sodium succinate. Throughout the four-week intervention period, mouse caloric intake was measured, as well as changes in body weight and body composition (fat mass and fat-free mass). Caloric intake was determined on the basis of the energy density of the diet (5.24 kcal/g). Energy density of accumulated fat mass in mice was 9.4 kcal/g and fat-free mass was 1.8 kcal/g[42]. On the basis of bomb calorimetry of faeces during the experiment, which found no differences in caloric absorption between interventions, we confirmed that the calculated metabolizable energy intake based on caloric intake measurements adequately accounted for any differences due to digestion.

High-fat feeding. All mouse high-fat feeding experiments were performed with age-matched littermate controls. At eight weeks of age, mice were switched to high-fat diet (OpenSource Diets, D12492) with 60% calories from fat, 20% calories from carbohydrate and 20% calories from protein. Following initiation of high-fat feeding, succinate in drinking water was added in the form of sodium succinate. Succinate-containing drinking water was freshly prepared and replaced every two days.

Body composition analysis. Body composition was examined with Echo MRI (Echo Medical Systems, Houston, Texas) using the 3-in-1 Echo MRI Composition Analyzer.

GTT. Mice were fasted for 6 h. Glucose (1 g/kg) was administered intraperitoneally, and blood glucose levels were measured at 0, 15, 30, 45, 60, 75, 90 and 120 min using a glucometer.

Bomb calorimetry of faeces. Calorimetry was conducted using a Parr 6725EA Semimicro Calorimeter and 1107 Oxygen Bomb. During dietary intervention, faecal specimens from mice were collected over a 48-h period. Collected samples were baked at 60 °C for 48 h to remove water content. Faecal samples were combusted and the energy content of the faecal matter was measured as heat of combustion (kcal/g).

Assessment of respiration in isolated mitochondria. BAT mitochondria were isolated as described previously[37]. Using freshly isolated mitochondria, basal respiration was measured in the presence of 10 mM pyruvate and 10 mM malate in the presence of 3 mM GDP in 50 mM KCl, 10 mM TES, 1mM EGTA medium containing 0.4% (w/v) fatty acid-free bovine serum albumin, 1 mM KH_2PO_4, 2 mM $MgCl_2$ and 0.46 mM $CaCl_2$. OCR was monitored in a Seahorse XF24 instrument at 2.5 μg mitochondrial protein per well. Succinate was added acutely at 5 mM following determination of basal respiration, leak was determined using 1 μg ml^{-1} oligomycin. 0.1 mM DNP was applied to determine chemically uncoupled respiration.

Histological analysis. Tissues were extracted and placed in tissue clamps in 10% neutral buffer formalin (NBF) overnight. The following day, samples were rinsed twice in PBS and stored in 70% ethanol. Tissue fragments were embedded in paraffin, sectioned and mounted on glass slides. For histological and morphometric studies, the sections were stained with haematoxylin and eosin or Masson's trichrome. Digital images were collected with a Nikon Ti2 motorized inverted microscope equipped with a 4× or 40× objective lens. Images were acquired with a Nikon DS-Fi1 colour camera controlled with NIS-Elements image acquisition software. The quantitative analysis of cardiomyocyte cross-sectional height and width and nuclear diameter were measured using Fiji image processing software.

Gene expression analysis. Total RNA was extracted from frozen tissue using TRIzol (Invitrogen), purified with a PureLink RNA Mini Kit (Invitrogen) and quantified using a Nanodrop 2000 UV–visible spectrophotometer. cDNA was prepared using 1 μg total RNA by a reverse transcription–polymerase chain

reaction (RT–PCR) using a high capacity cDNA reverse transcription kit (Applied Biosystems), according to the manufacturer's instructions. Real-time quantitative PCR (qPCR) was performed on cDNA using SYBR Green probes. qPCR was performed on a 7900 HT Fast Real-Time PCR System (Applied Biosystems) using GoTaq qPCR Master Mix (Promega). Reactions were performed in a 384-well format using an ABI PRISM 7900HT real time PCR system (Applied Biosystems). For SYBR primer pair sequences see Supplementary Methods. Fold changes in expression were calculated by the $\Delta\Delta C_t$ method using mouse cyclophilin A as an endogenous control for mRNA expression. All fold changes are expressed normalized to the vehicle control. SYBR primer pair sequences were as follows. *Il1b*: forward, 5′-TGGCAACTGTTCCTG-3′; reverse, 5′-GGAAGCAGCCCTTCATCTTT-3′; *Il10*: forward, 5′-AGGCGCTGTCATCG-ATTT-3′; reverse, 5′-CACCTTG GTCTTGGAGCTTAT-3′; *Tnfa*: forward, 5′-GCCTCTTCT-CATTCC TGCTT-3′; reverse, 5′-TGGGAACTTCTCATCCCTTTG-3′; *Arg1*: forward, 5′-GATTATCGGAGCGCCTTTCT-3′; reverse, 5′-TGGTCTCTCACGTCA TACTCT-3′; *Nos2*: forward, 5′-CCAAGCCCTCACCTACTTCC-3′; reverse, 5′- CTCTGAGGGCTGACACAAGG-3′; *Il6*: forward, 5′-ACAAAGCCAGAGTCC TTCAGAGAG-3′; reverse, 5′-TTGGATGGTCTTGGTCCTTAGCCA-3′; *Mrc1*: forward, 5′-GGCGAGCATCAAGAGTAAAGA-3′; reverse, 5′-CATAGGTC AGTCCCAACCAAA-3′; cyclophilin (*Ppia*): forward, 5′-GGAGATGG CACAGGAGGAA-3′; reverse, 5′- GCCCGTAGTGCTTCAGCTT-3′.

Statistical analyses. Data were expressed as mean ± s.e.m. and *P* values were calculated using two-tailed Student's *t*-test for pairwise comparison of variables, one-way ANOVA for multiple comparison of variables, and two-way ANOVA for multiple comparisons involving two independent variables. Sample sizes were determined on the basis of previous experiments using similar methodologies. For all experiments, all stated replicates are biological replicates. For in vivo studies, mice were randomly assigned to treatment groups. For mass spectrometry analyses, samples were processed in random order and experimenters were blinded to experimental conditions.

Reporting summary. Further information on experimental design is available in the Nature Research Reporting Summary linked to this paper.

Data availability. Full scans for all western blots are provided in Supplementary Information. Source Data for all mouse experiments have been provided. All other data are available from the corresponding author on reasonable request.

32. Pan, D., Fujimoto, M., Lopes, A. & Wang, Y. X. Twist-1 is a PPARδ-inducible, negative-feedback regulator of PGC-1α in brown fat metabolism. *Cell* **137**, 73–86 (2009).
33. Cannon, B. & Nedergaard, J. Nonshivering thermogenesis and its adequate measurement in metabolic studies. *J. Exp. Biol.* **214**, 242–253 (2011).
34. Gospodarska, E., Nowialis, P. & Kozak, L. P. Mitochondrial turnover: a phenotype distinguishing brown adipocytes from interscapular brown adipose tissue and white adipose tissue. *J. Biol. Chem.* **290**, 8243–8255 (2015).
35. Townsend, M. K. et al. Reproducibility of metabolomic profiles among men and women in 2 large cohort studies. *Clin. Chem.* **59**, 1657–1667 (2013).
36. Kir, S. et al. Tumour-derived PTH-related protein triggers adipose tissue browning and cancer cachexia. *Nature* **513**, 100–104 (2014).
37. Kazak, L. et al. A creatine-driven substrate cycle enhances energy expenditure and thermogenesis in beige fat. *Cell* **163**, 643–655 (2015).
38. Shinoda, K. et al. Genetic and functional characterization of clonally derived adult human brown adipocytes. *Nat. Med.* **21**, 389–394 (2015).
39. Eng, J. K., McCormack, A. L. & Yates, J. R. An approach to correlate tandem mass spectral data of peptides with amino acid sequences in a protein database. *J. Am. Soc. Mass Spectrom.* **5**, 976–989 (1994).
40. Elias, J. E. & Gygi, S. P. Target-decoy search strategy for increased confidence in large-scale protein identifications by mass spectrometry. *Nat. Methods* **4**, 207–214 (2007).
41. Huttlin, E. L. et al. A tissue-specific atlas of mouse protein phosphorylation and expression. *Cell* **143**, 1174–1189 (2010).
42. Guo, J. & Hall, K. D. Predicting changes of body weight, body fat, energy expenditure and metabolic fuel selection in C57BL/6 mice. *PLoS One* **6**, e15961 (2011).

a

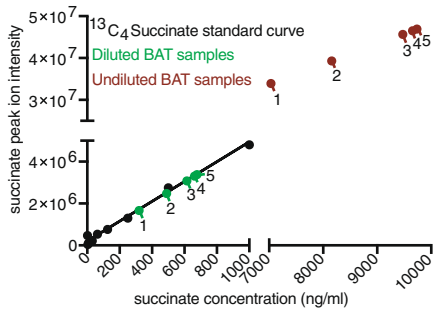

b

succinate sample	apparent dilution	actual dilution
1	28	100
2	13.7	100
3	14.8	100
4	14.2	100
5	11.6	100

Extended Data Fig. 1 | Quality control for mass-spectrometry analysis of succinate in thermogenic adipose tissue. a, Because of its unusual abundance in BAT, special consideration is required to determine the linearity of the relationship between LC–MS succinate peak intensity and succinate concentration for quantitative analysis. Succinate abundance is measured in extraction solution as described in the methods section. Absolute determination of succinate concentration is compared between succinate extracted from BAT (red) and the same samples following 100-fold dilution (green). Samples are analysed in parallel with defined amounts of [^{13}C]succinate (black) used at concentrations that are within the established linear range of the mass spectrometer. Following 100-fold dilution of BAT extracts, succinate signals are within the linear range of detection. However, undiluted extracts are at concentrations that result in a nonlinear relationship and are therefore not appropriate for quantitative analysis. **b**, Calculation of the apparent dilution factor reveals the effect of nonlinearity with apparent dilutions ranging from ~11–28-fold that are in fact 100-fold.

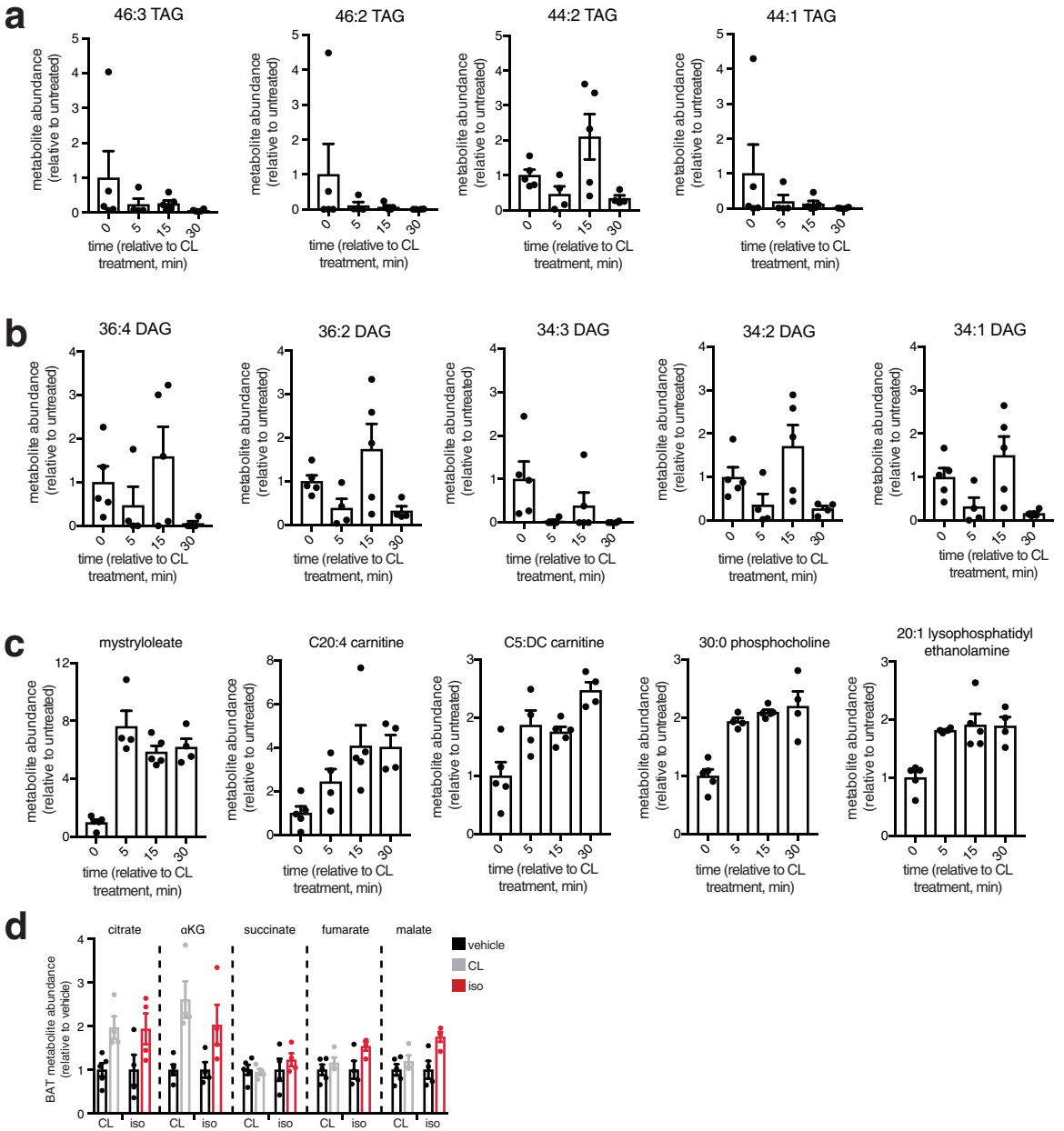

Extended Data Fig. 2 | Metabolite analysis of the acute response of BAT to β-adrenergic stimulus in vivo. a, **b**, Rapid modulation of BAT triacylglycerol (TAG; **a**) and diacylglycerol (DAG; **b**) species following intravenous injection of 1 mg kg^{-1} CL. **c**, Accumulation of free fatty acid species and acyl-carnitine species in BAT following intravenous injection of CL. **d**, Abundance of TCA cycle metabolites in BAT following intravenous β-adrenoreceptor agonism with 1 mg kg^{-1} isoproterenol or 1 mg kg^{-1} CL ($n = 5$; CL, iso, $n = 4$). **c**, One-way ANOVA; **d**, two-sided *t*-test; data are mean ± s.e.m. of biologically independent samples.

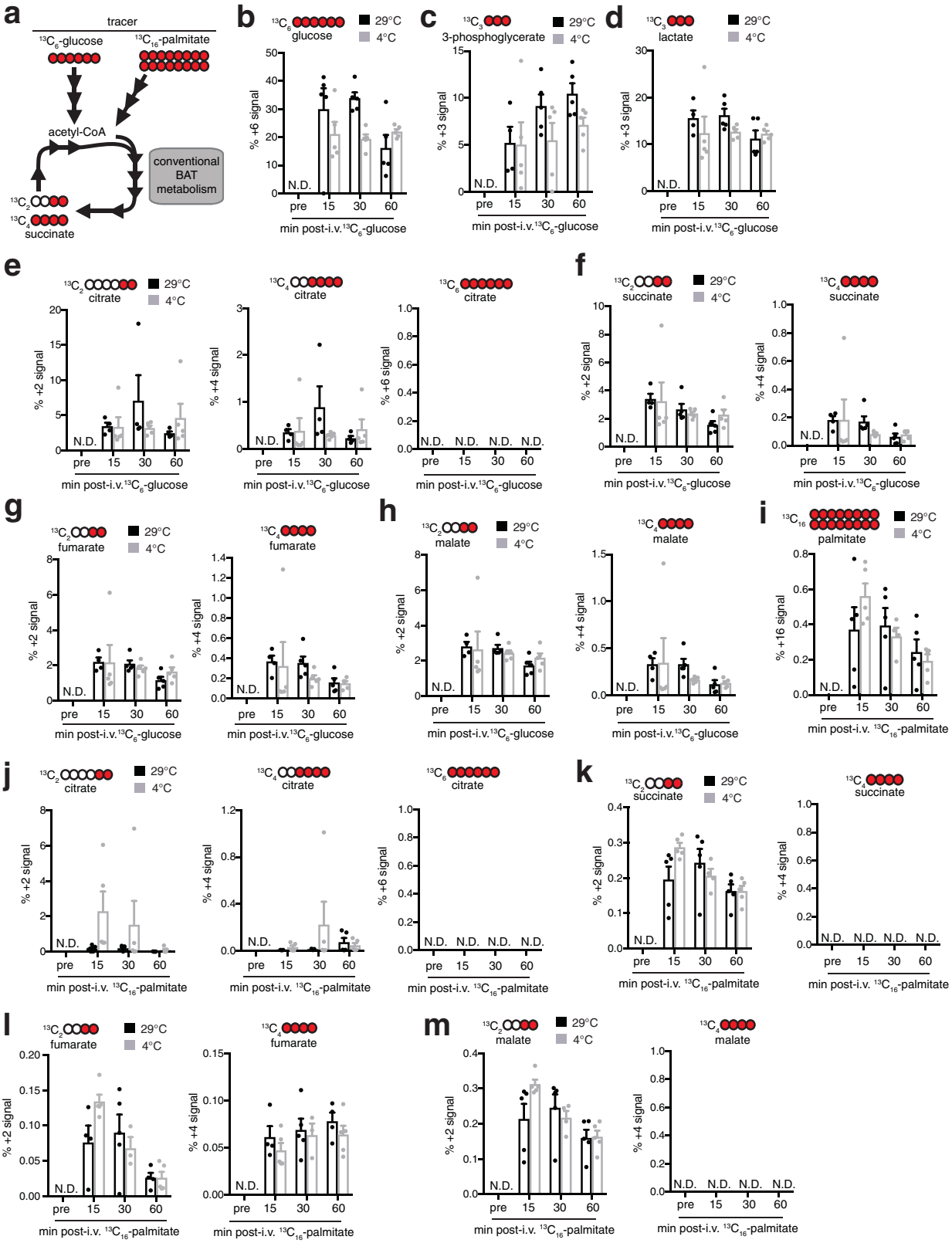

Extended Data Fig. 3 | ^{13}C-isotopologue labelling of glucose and TCA cycle metabolites in mouse BAT following intravenous [^{13}C] glucose at 29 °C or 4 °C. a, Potential inputs to succinate-directed flux by conventional BAT metabolism and ^{13}C-metabolite labelling strategy. Mice were administered [U-^{13}C]glucose (**b**–**h**) or [U-^{13}C]palmitic acid (**i**–**m**) intravenously as a bolus at 29 °C or 4 °C followed by BAT harvesting and snap freezing for LC–MS analysis at indicated time points. **b**, Proportional isotopic labelling of BAT glucose. **c**, **d**, Proportional isotopic labelling profile of glycolytic metabolites 3-phosphoglycerate (**c**) and lactate (**d**) in mouse BAT. **e**–**h**, Proportional isotopic labelling profile of TCA cycle metabolites citrate (**e**), succinate (**f**), fumarate (**g**), and malate (**h**) in mouse BAT. **i**, Proportional isotopic labelling of BAT palmitate. **j**–**m**, Proportional isotopic labelling profile of TCA cycle metabolites citrate (**j**), succinate (**k**), fumarate (**l**), and malate (**m**) in BAT ($n = 5$). Missing values or N.D. indicate value not determined. Data are mean ± s.e.m. of biologically independent samples.

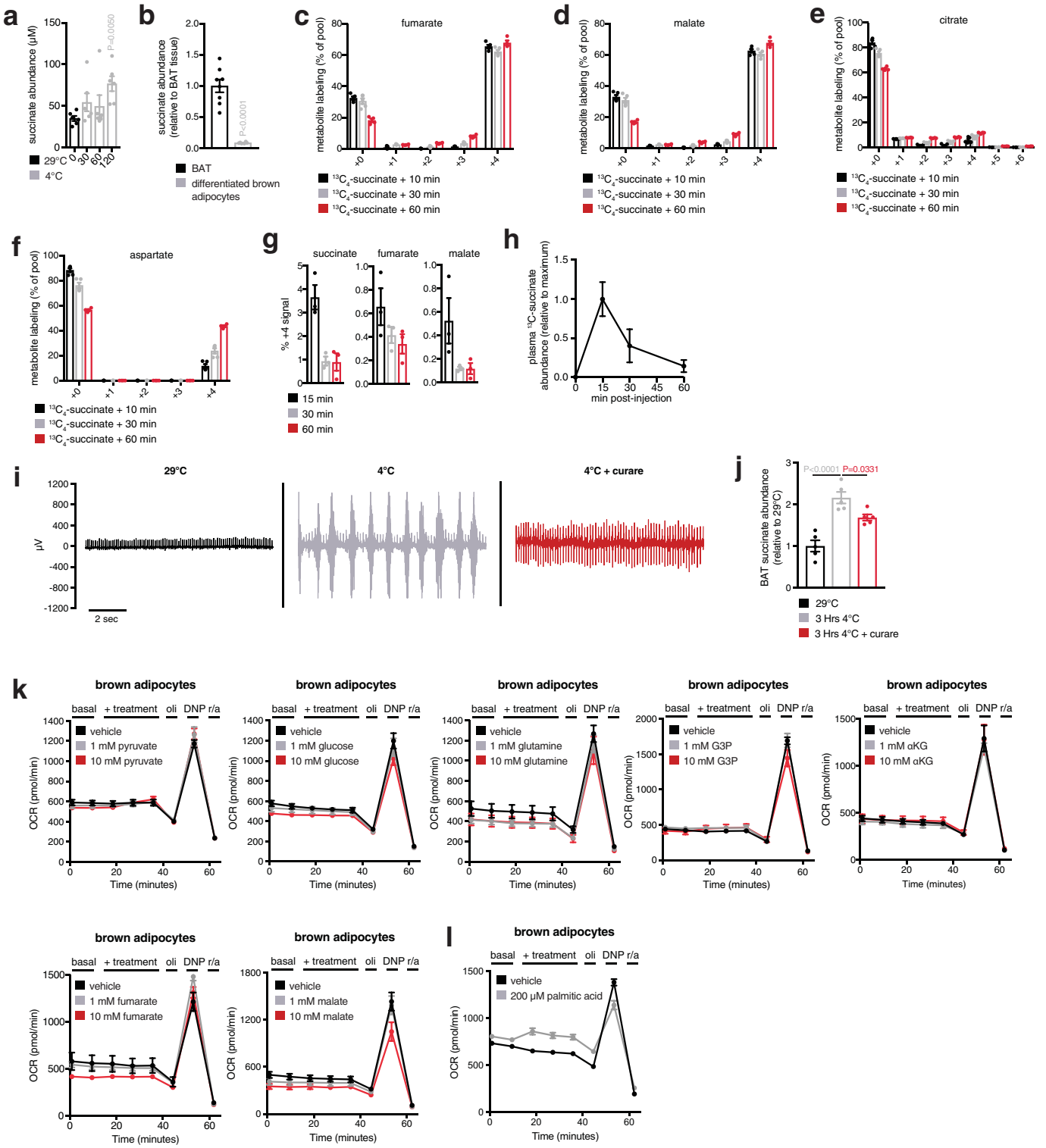

Extended Data Fig. 4 | See next page for caption.

Extended Data Fig. 4 | Analysis of succinate levels in isolated brown adipocytes and effect of muscle shivering on BAT succinate accumulation. a, Abundance of succinate in mouse plasma comparing 29 °C to acute 4 °C exposure ($n = 6$). **b**, Comparison of succinate abundance in BAT in vivo ($n = 8$) versus brown adipocytes ($n = 7$). **c**–**f**, Full ^{13}C-isotopologue profile of fumarate (**c**), malate (**d**), citrate (**e**), and aspartate (**f**) in brown adipocytes following extracellular addition of [^{13}C]succinate ($n = 5$). **g**, ^{13}C-isotopologue ($m + 4$) profile of TCA metabolites downstream of mitochondrial succinate oxidation in BAT following intravenous administration of 100 mg kg^{-1} [^{13}C]succinate as a bolus ($n = 3$). **h**, Time course of abundance of ($m + 4$) [^{13}C]succinate in plasma following 100 mg kg^{-1} intravenous [^{13}C]succinate ($n = 3$, except 15 min, $n = 4$). **i**, Representative mouse nuchal muscle EMG traces at 29 °C and after acute cold exposure with or without curare (0.1 mg kg^{-1}). **j**, Quantification of succinate in BAT at 29 °C and after acute cold exposure with or without inhibition of muscle shivering with curare (0.1 mg kg^{-1}; $n = 5$). **k**, Effect of acute addition of cellular and mitochondrial respiratory substrates on brown adipocyte respiration. Pyruvate: vehicle, $n = 7$; 1 mM, $n = 6$; 10 mM, $n = 7$; glucose: vehicle, $n = 7$; 1 mM, $n = 6$; 10 mM, $n = 7$; glutamine: vehicle, $n = 6$; 1 mM, $n = 6$; 10 mM, $n = 7$; G3P: vehicle, $n = 7$; 1 mM, $n = 6$; 10 mM, $n = 6$; αKG: vehicle, $n = 6$; 1 mM, $n = 6$; 10 mM, $n = 5$; fumarate: vehicle, $n = 6$; 1 mM, $n = 6$; 10 mM, $n = 5$; malate: vehicle, $n = 6$; 1 mM, $n = 6$; 10 mM, $n = 7$. **l**, Effect of acute addition of palmitic acid on brown adipocyte respiration (vehicle, $n = 18$; palmitic acid, $n = 16$). Effects on respiration were determined by acute addition of oligomycin (oli) to determine leak respiration, 2,4-dinitrophenol (DNP) to determine chemically uncoupled maximal respiration, and rotenone plus antimycin (r/a) to determine non-mitochondrial respiration. In all cases basal respiration in these cells is measured in the presence of 1 mM pyruvate. One-way ANOVA (**a**, **j**); data are mean ± s.e.m. of biologically independent samples.

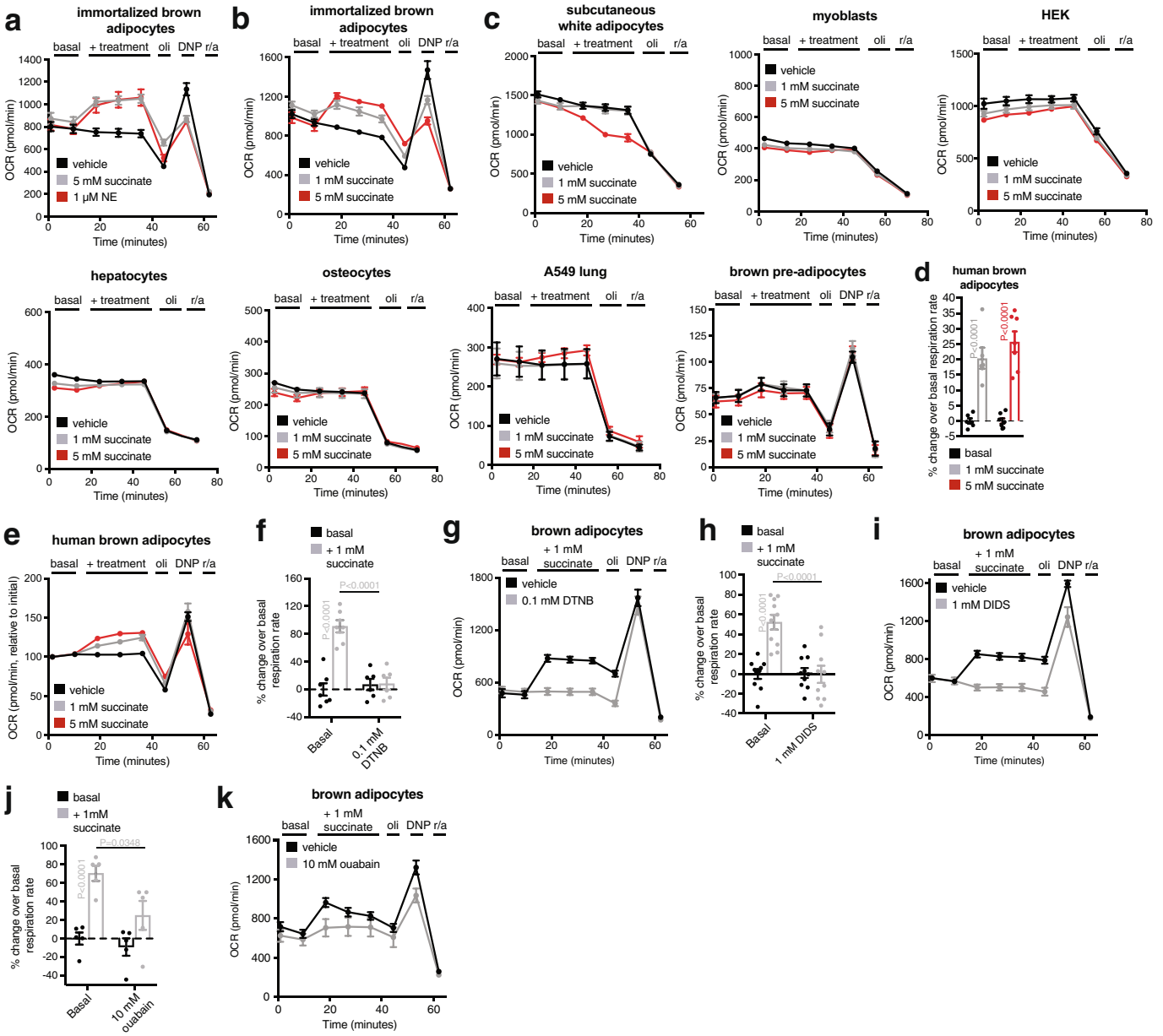

Extended Data Fig. 5 | Representative OCR experiments for brown adipocytes and other cell types with or without acute addition of succinate and related substrates. a, Representative OCR trace monitoring effect of acute addition of succinate or noradrenaline (NE) in the De2.3 immortalized brown adipocyte cell line[32] (vehicle, $n=7$; succinate, $n=6$; NE, $n=7$). **b**, Representative OCR trace monitoring dose-dependent effect of acute addition of succinate in the De2.3 immortalized brown adipocyte cell line (vehicle, $n=7$; 1 mM succinate, $n=6$; 5 mM succinate, $n=7$). **c**, Representative OCR trace monitoring dose-dependent effect of acute addition of succinate in various cell types (subcutaneous white adipocytes: vehicle, $n=6$; 1 mM, $n=6$; 5 mM, $n=5$; myoblasts: vehicle, $n=7$; 1 mM, $n=6$; 5 mM, $n=7$; HEK: vehicle, $n=7$; 1 mM, $n=6$; 5 mM, $n=7$; hepatocytes: vehicle, $n=7$; 1 mM, $n=6$; 5 mM, $n=7$; osteocytes: vehicle, $n=7$; 1 mM, $n=6$; 5 mM, $n=7$; A549 lung: vehicle, $n=7$; 1 mM, $n=6$; 5 mM, $n=7$; brown pre-adipocytes: vehicle, $n=7$; 1 mM, $n=6$; 5 mM, $n=7$). **d**, Effect of acute addition of succinate on cellular OCR in human brown adipocytes (basal, $n=6$; 1 mM, $n=6$; 5 mM, $n=7$). **e**, Representative OCR trace monitoring dose-dependent effect of acute addition of succinate in human immortalized brown adipocytes (vehicle, $n=7$; 1 mM succinate, $n=6$; 5 mM succinate, $n=7$). **f**, Inhibition of succinate-stimulated OCR in brown adipocytes by DTNB. **g**, Representative OCR experiment ($n=7$; 0.1 mM DTNB, $n=6$). **h**, **i**, Inhibition of succinate-stimulated OCR in brown adipocytes by DIDS. $n=12$, except 1 mM DIDS, $n=8$). **j**, **k**, Inhibition of succinate-stimulated OCR in brown adipocytes by treatment with the Na^+/K^+ ATPase inhibitor ouabain ($n=5$). Effects on respiration were determined by acute addition of oligomycin (oli) to determine leak respiration, 2,4-dinitrophenol (DNP) to determine chemically uncoupled maximal respiration, or rotenone plus antimycin (r/a) to determine non-mitochondrial respiration. In all cases basal respiration in these cells is measured in the presence of 1 mM pyruvate. Two-sided *t*-test (**d**); two-way ANOVA (**f**, **h**, **j**); data are mean ± s.e.m. of biologically independent samples.

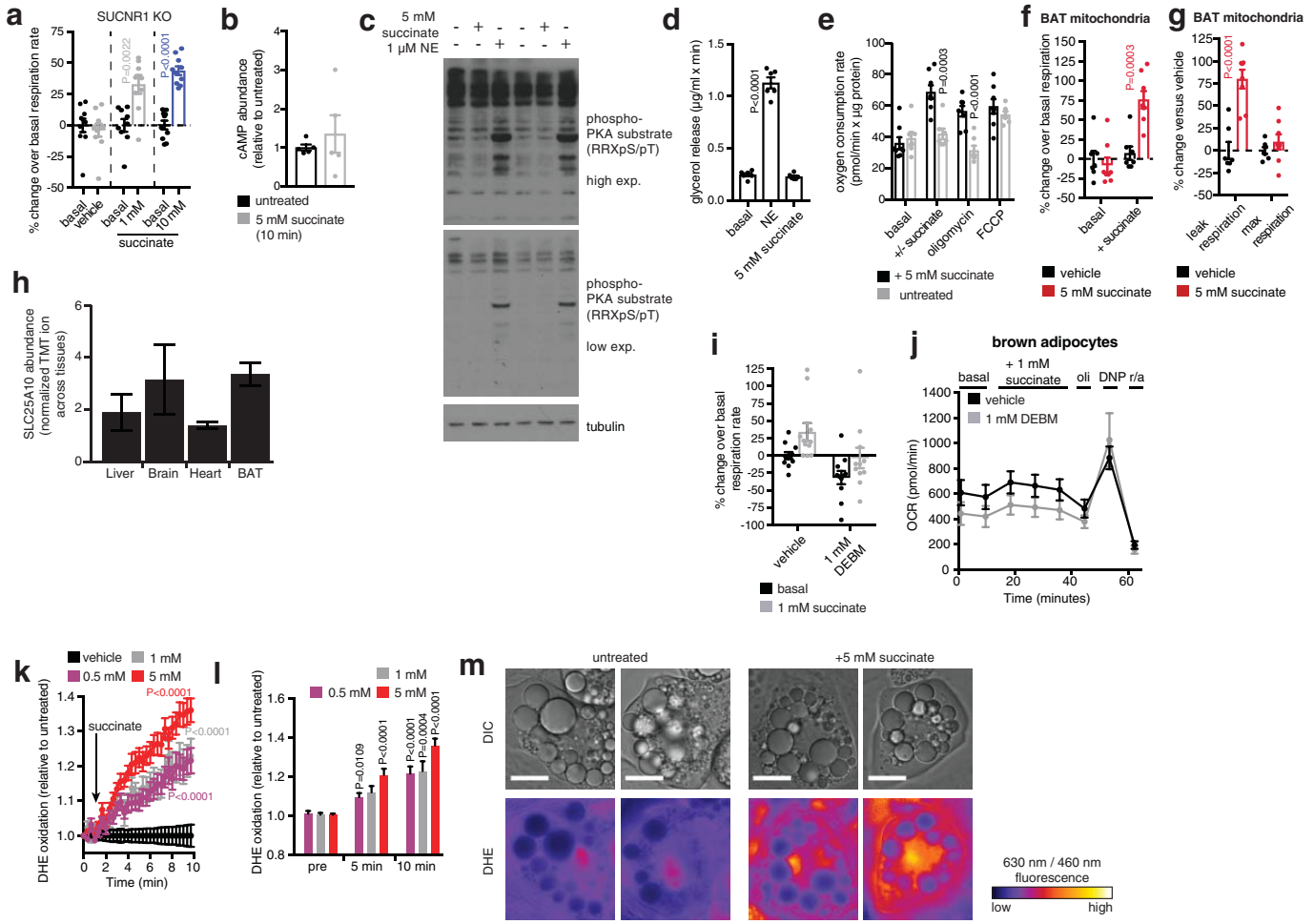

Extended Data Fig. 6 | Examining mechanisms of succinate-driven thermogenesis in brown adipocytes. a, Succinate-induced respiration is intact in brown adipocytes lacking SUCNR1 ($n = 10$, except 1 mM succinate, $n = 9$). **b**, Measurement of cAMP in brown adipocytes 10 min following addition of succinate. **c**, Immunoblot analysis of PKA substrate phosphorylation following addition of succinate (30 min) or NE (5 min). **d**, Glycerol release rate from brown adipocytes as an index of lipolysis in response to succinate or NE ($n = 6$). **e**–**g**, Effect of acute addition of succinate in mitochondria isolated from BAT, monitoring effects on basal respiration rate (**f**), leak respiration (**g**), and chemically uncoupled maximal respiration (**g**). $n = 7$, except succinate, $n = 8$). **h**, Quantitation of SLC25A10 protein levels in mouse liver, brain, heart, and BAT ($n = 3$). **i**, **j**, Inhibition of succinate-stimulated OCR in brown adipocytes by treatment with the SLC25A10 inhibitor diethyl butylmalonate (DEBM; $n = 11$). Data are mean ± s.e.m. of at least three replicates. **k**, Effect of succinate treatment on ROS levels in brown adipocyte assessed by DHE oxidation ($n = 15$). **l**, Acute addition of succinate drives rapid DHE oxidation in brown adipocytes ($n = 15$). **m**, Representative high resolution microscopy images illustrating effect of acute (10 min) addition of succinate on DHE oxidation in brown adipocytes. Scale bars, 20 μm. Two-sided *t*-test (**a**, **e**, **f**, **g**); one-way ANOVA (**d**, **l**); two-way ANOVA (**k**); data are mean ± s.e.m. of biologically independent samples.

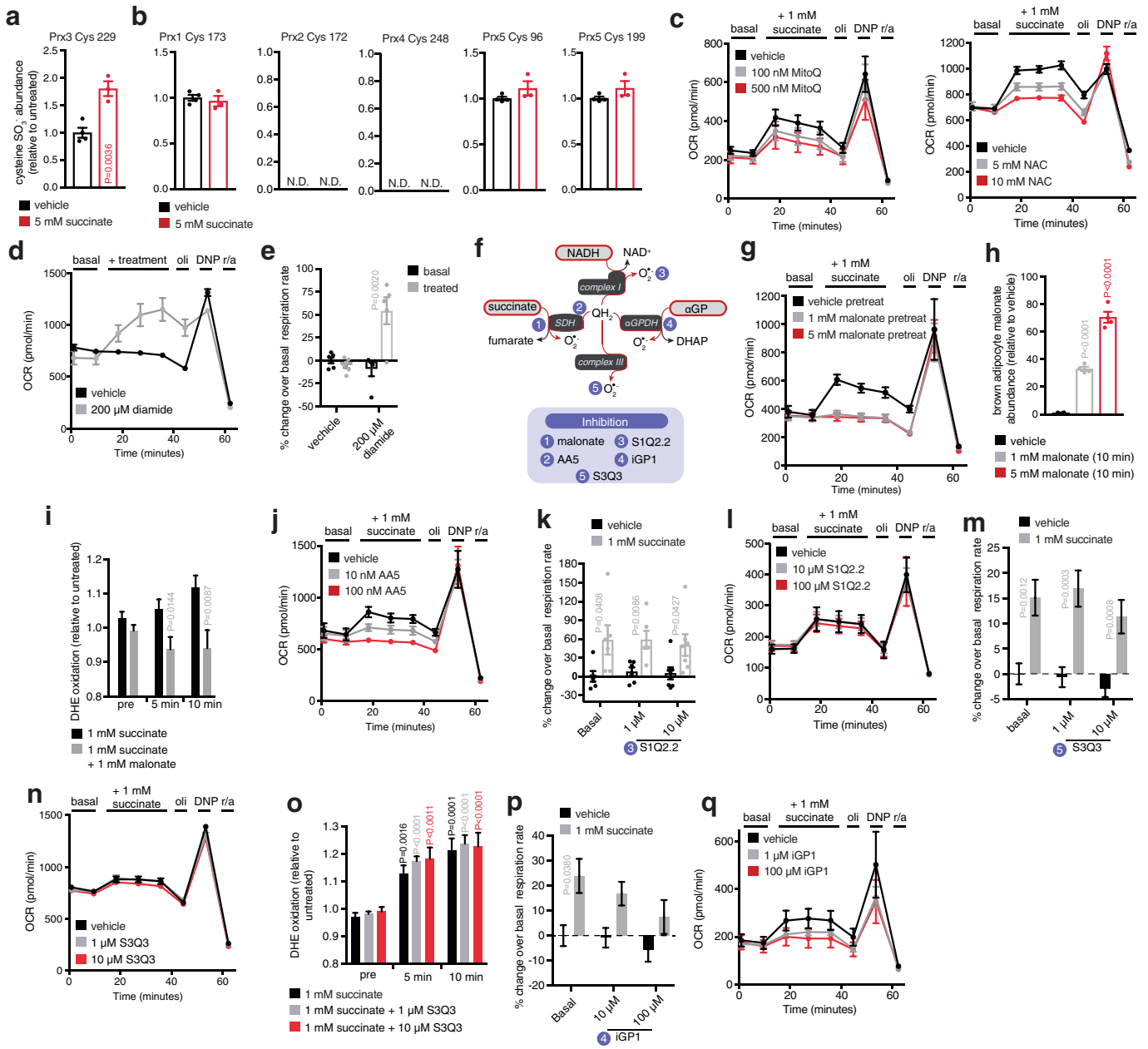

Extended Data Fig. 7 | Mechanisms of succinate-driven thermogenic ROS and respiration in brown adipocytes. a, Effect of succinate treatment on Prx3 cysteine-thiol sulfonic acid formation (vehicle, $n = 4$; succinate, $n = 3$). **b**, Effect of succinate treatment on Prx family cysteine-thiol sulfonic acid (SO_3^-) status (vehicle, $n = 4$; succinate, $n = 3$). **c**, Representative OCR experiments on brown adipocytes with or without acute added succinate with or without MitoQ or NAC. Effects on respiration were determined by acute addition of oligomycin (oli) to determine leak respiration, DNP to determine chemically uncoupled maximal respiration, and rotenone plus antimycin (r/a) to determine non-mitochondrial respiration (MitoQ: vehicle, $n = 6$; 100 nM, $n = 6$; 500 nM, $n = 5$; NAC: vehicle, $n = 7$; 5 mM, $n = 6$; 10 mM, $n = 7$). **d**, **e**, Representative OCR experiments on brown adipocytes with and without acute addition of diamide. Vehicle, $n = 6$; 200 μM diamide, $n = 5$. **f**, Potential pathways for succinate-driven thermogenic ROS in brown adipocytes via SDH or electron transfer via ubiquinol (QH_2): (1) Malonate inhibits succinate oxidation by SDH[19]; (2) atpenin A5 (AA5) inhibits electron transfer between SDH and the ubiquinone pool[20]; (3) S1Q2.2 inhibits ROS production from mitochondrial complex I[21]; (4) iGP1 inhibits electron transfer between αGPDH and the ubiquinone pool[23]; and (5) S3Q3 inhibits ROS production from mitochondrial complex III[22]. **g**, Representative OCR experiment demonstrating inhibition of succinate stimulated OCR by suppression of SDH oxidation with malonate (vehicle, $n = 6$; 1 mM malonate, $n = 6$; 5 mM malonate, $n = 5$). **h**, **i**, Treatment of brown adipocytes with malonate results in rapid intracellular accumulation ($n = 4$) (**h**) and prevents succinate-driven DHE oxidation (**i**) in brown adipocytes ($n = 30$). **j**–**l**, Representative OCR experiments in brown adipocytes with or without acute addition of succinate, with or without AA5 (**j**; vehicle, $n = 6$; 10 nM, $n = 6$; 100 nM, $n = 5$); S1Q2.2 (**k**, **l**; vehicle, $n = 6$; 10 μM, $n = 6$; 100 μM, $n = 7$); S3Q3 (**m**, **n**; vehicle, $n = 13$; 1 μM $n = 12$; 10 μM $n = 13$). **o**, Treatment of brown adipocytes with S3Q3 has no effect on succinate-driven DHE oxidation in brown adipocytes ($n = 30$, except 1 μM, $n = 15$). **p**, Succinate stimulation of brown adipocyte OCR with or without iGP(iGP vehicle, $n = 21$; 10 μM iGP, $n = 17$; 100 μM iGP, $n = 26$). **q**, Representative OCR experiments in brown adipocytes with or without acute addition of succinate and/or iGP1 (vehicle, $n = 7$; 1 μM, $n = 6$; 100 μM, $n = 7$). Two-sided *t*-test (**a**, **e**, **i**); one-way ANOVA (**h**, **o**); two-way ANOVA (**k**, **m**, **p**); data are mean ± s.e.m. of biologically independent samples.

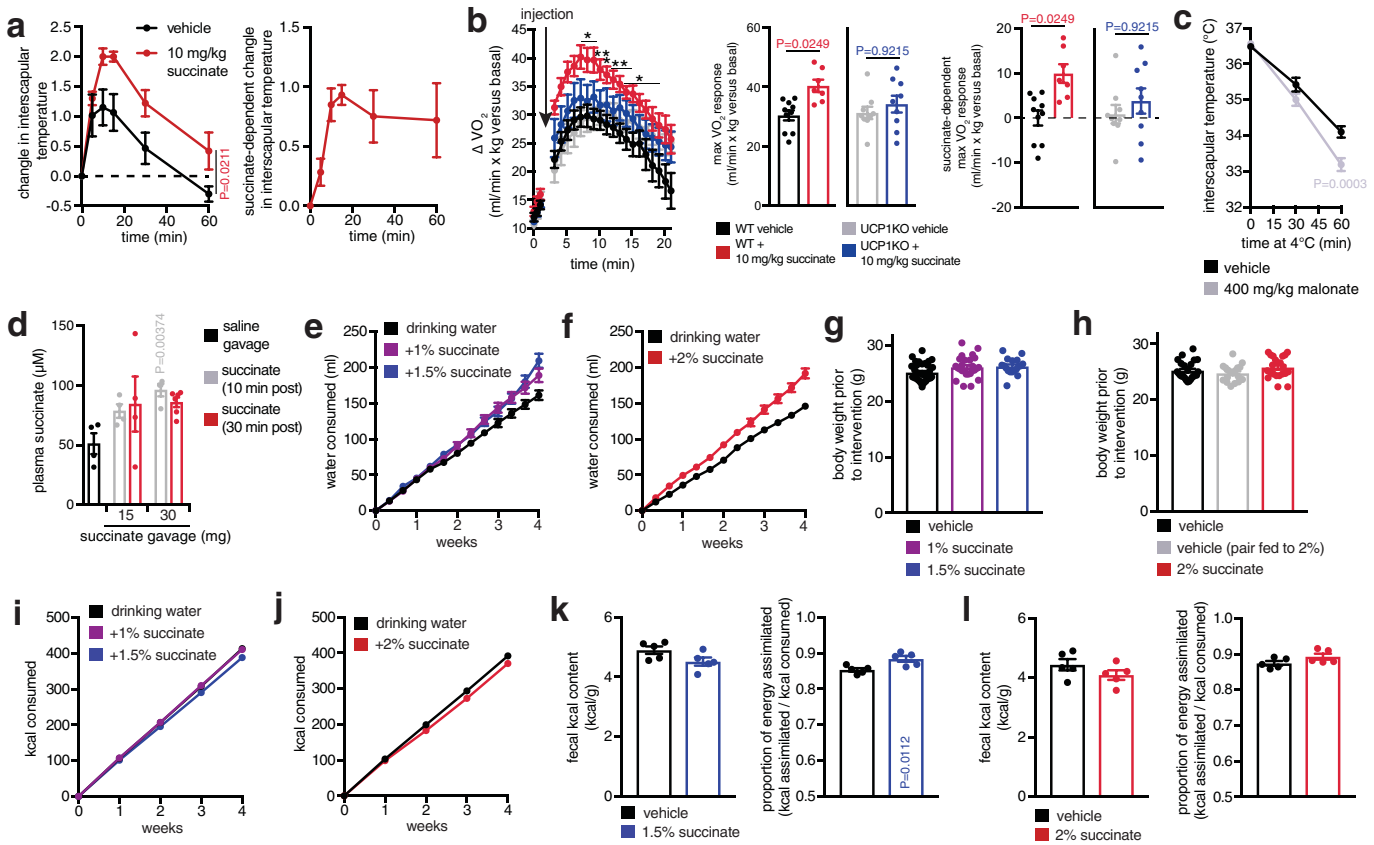

Extended Data Fig. 8 | Metabolic characterization of mice following systemic succinate administration. a, Effect of acute intravenous administration of succinate on interscapular temperature (vehicle, $n = 6$; succinate, $n = 5$). **b**, Acute effect of intravenous succinate on whole body oxygen consumption in wild-type (WT) and UCP1(KO) mice. Basal O_2 consumption rate determined as described in the Methods (vehicle, $n = 10$; succinate, $n = 7$; UCP1(KO), $n = 9$). **c**, Mouse interscapular temperature following acute exposure to 4 °C with or without acute intravenous administration of malonate ($n = 8$). Malonate was administered 10 min before transition to 4 °C. **d**, Acute oral administration of succinate by gavage drives elevation of circulating succinate ($n = 4$, except 10% 30 min, $n = 6$). **e**, Water consumption during high-fat feeding with or without intervention with 1% and 1.5% sodium succinate in drinking water indicates lack of aversion to succinate-containing water (vehicle, $n = 35$; 1%, $n = 26$; 1.5%, $n = 18$). **f**, Water consumption during high-fat feeding with or without intervention with 2% succinate in drinking water indicates lack of aversion to succinate-containing water (vehicle, $n = 24$; 2%, $n = 22$). **g**, Body weights of high-fat diet feeding mice before intervention with 1% and 1.5% sodium succinate in drinking water (vehicle, $n = 35$; 1%, $n = 26$; 1.5%, $n = 18$). **h**, Body weights of high-fat diet feeding mice before intervention with 2% sodium succinate in drinking water (vehicle, $n = 24$; 2%, $n = 22$; pair fed, $n = 18$). **i**, Caloric consumption during high-fat feeding with or without intervention with 1% or 1.5% sodium succinate in drinking water (vehicle, $n = 35$; 1%, $n = 26$; 1.5%, $n = 18$). **j**, Caloric consumption during high-fat feeding with or without 2% sodium succinate in drinking water, pair-fed mice in this experiment were fed the same number of calories as the 2% succinate group (vehicle, $n = 24$; 2%, $n = 22$; pair fed, $n = 18$). **k**, **l**, Caloric absorption and energy assimilation during high-fat feeding with or without 1.5% (**k**) or 2% (**l**) sodium succinate in drinking water. Proportion of energy assimilated from diet was determined by subtracting the total calories remaining in mouse faeces from the total calories consumed in the same period ($n = 6$). $^*P < 0.05$, $^{**}P < 0.01$; two-way ANOVA (**a**, **b** (left), **c**); one-way ANOVA (**b** (middle, right), **d**); two-sided *t*-test (**k**); data are mean ± s.e.m. of biologically independent samples.

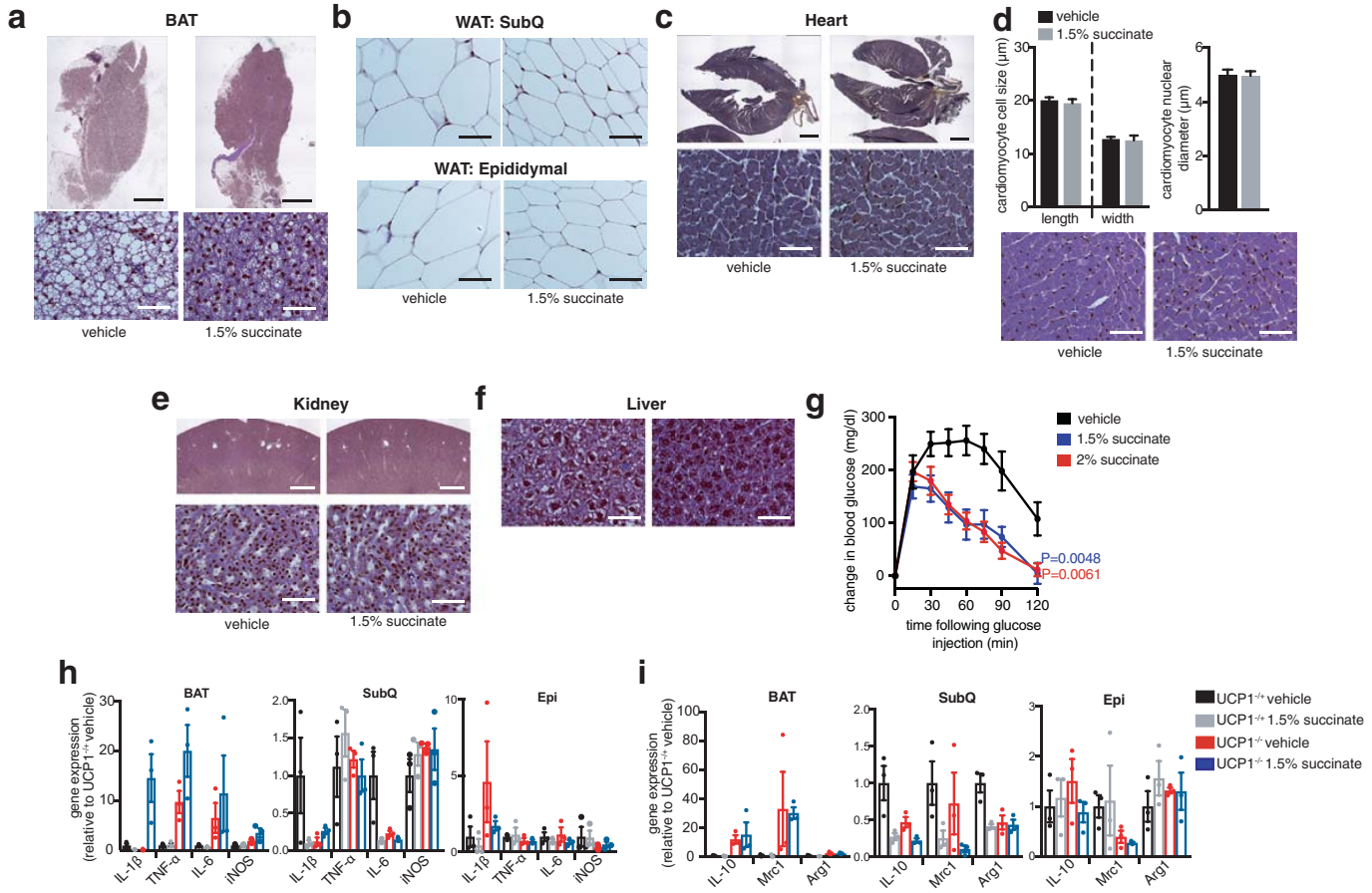

Extended Data Fig. 9 | Assessment of morphologic effects of systemic succinate administration on mouse tissues. a–**f**, Representative images of haematoxylin and eosin (**a**, **b**, **d**–**f**) or Masson's trichrome (**c**) staining of indicated tissues harvested from mice following high-fat feeding with or without 4 weeks succinate supplementation in drinking water. (**a**, **c**, **e** top panels: 4× magnification; scale bars, 1 mm; **a**, **c**, **e** bottom panels, **b**, **d**, **f**: 40× magnification, scale bars, 50 μm). **d**, Cardiac morphometric analysis with or without 1.5% sodium succinate. Lower panels show representative images of cell width (40× magnification; scale bars, 50 μm). Bar charts show quantitative analysis of cardiomyocyte width and length and nuclear diameter ($n = 15$). **g**, Intraperitoneal glucose tolerance test in mice following high-fat feeding with or without 4 weeks succinate supplementation in drinking water, quantifying relative changes in glucose upon glucose challenge ($n = 9$). **h**, **i**, mRNA expression of inflammatory (**h**) and anti-inflammatory (**i**) markers in the indicated tissues with or without 1.5% sodium succinate in wild-type and *Ucp1*$^{-/-}$ mice ($n = 3$). Two-way ANOVA (**g**); one-way ANOVA (**h**); data are mean ± s.e.m. of biologically independent samples.

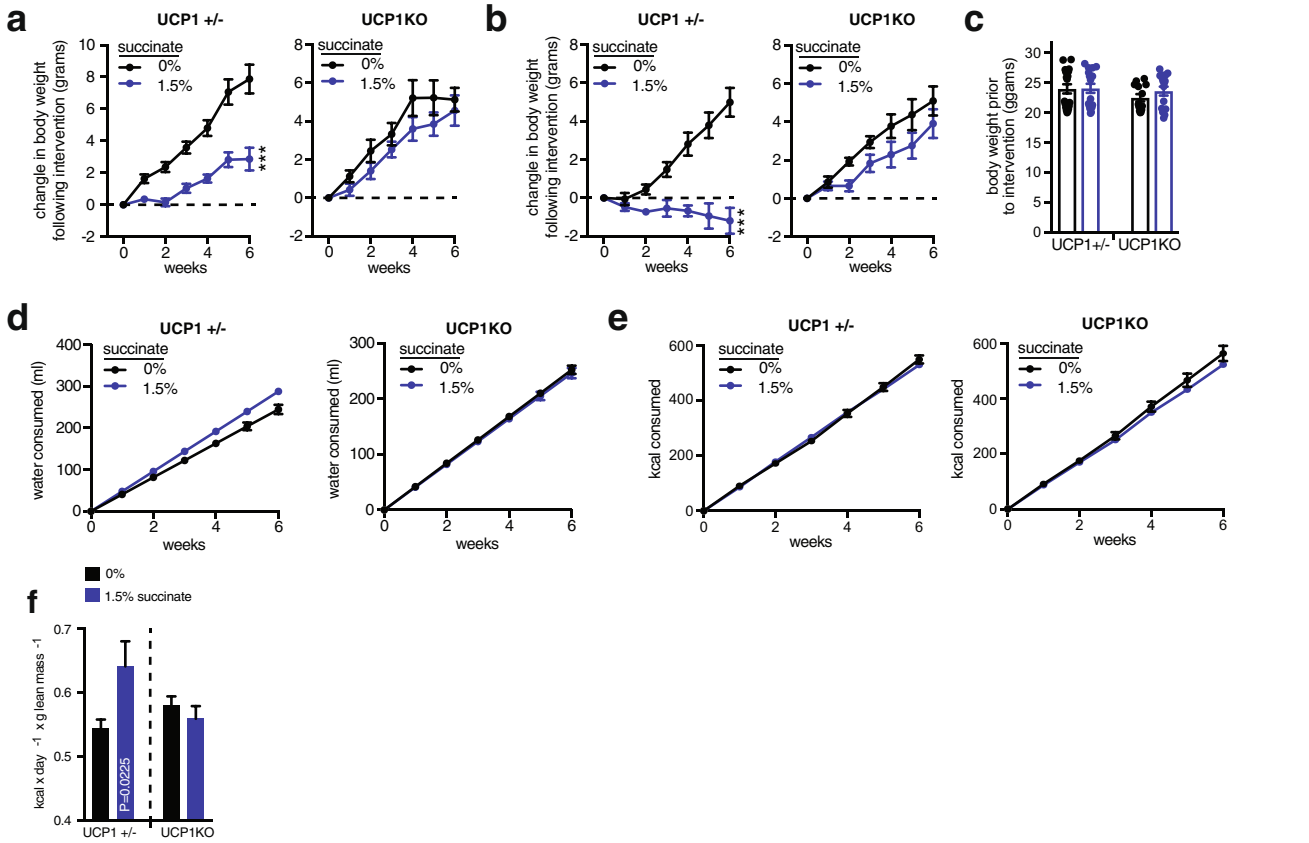

Extended Data Fig. 10 | Metabolic characterization of UCP1-deficient mice following systemic succinate administration. a, Change in body mass in $Ucp1^{+/-}$ ($n = 9$; 1.5% $n = 9$) and $Ucp1^{-/-}$ (UCP1KO, $n = 7$; 1.5% $n = 8$) male mice during high-fat feeding with or without 1.5% sodium succinate in drinking water. **b**, Change in body mass in $Ucp1^{+/-}$ (0%, $n = 9$; 1.5%, $n = 8$) and $Ucp1^{-/-}$ (0%, $n = 6$; 1.5% $n = 7$) female mice during high-fat feeding with or without 1.5% sodium succinate in drinking water. **c**, Body weights of high-fat diet feeding $Ucp1^{+/-}$ (vehicle, $n = 18$; 1.5%, $n = 17$) and $Ucp1^{-/-}$ (vehicle, $n = 13$; 1.5%, $n = 15$) mice prior to intervention with 1.5% sodium succinate in drinking water. **d**, Water consumption during high-fat feeding with or without intervention with 1.5% sodium succinate in drinking water in $Ucp1^{+/-}$ (0%, $n = 18$; 1.5%, $n = 17$) and $Ucp1^{-/-}$ (0%, $n = 13$; 1.5%, $n = 15$) mice indicates lack of aversion to succinate-containing water. **e**, Energy consumption during high-fat feeding with or without intervention with 1.5% sodium succinate in drinking water in $Ucp1^{+/-}$ (0%, $n = 18$; 1.5%, $n = 17$) and $Ucp1^{-/-}$ (0%, $n = 13$; 1.5%, $n = 15$) mice. **f**, Energy expenditure of $Ucp1^{+/-}$ and $Ucp1^{-/-}$ mice during 6 weeks high-fat feeding with or without 1.5% sodium succinate ($Ucp1^{+/-}$ 0%, $n = 18$; $Ucp1^{+/-}$ 1.5%, $n = 17$; $Ucp1^{-/-}$ 0%, $n = 13$; $Ucp1^{-/-}$ 1.5%, $n = 15$). Two-way ANOVA (**a**, **b**); one-way ANOVA (**f**); data are mean ± s.e.m. of biologically independent samples.

nature research

Corresponding author(s): Edward Thomas Chouchani

Reporting Summary

Nature Research wishes to improve the reproducibility of the work that we publish. This form provides structure for consistency and transparency in reporting. For further information on Nature Research policies, see Authors & Referees and the Editorial Policy Checklist.

Statistical parameters

When statistical analyses are reported, confirm that the following items are present in the relevant location (e.g. figure legend, table legend, main text, or Methods section).

n/a	Confirmed	
☐	☒	The exact sample size (*n*) for each experimental group/condition, given as a discrete number and unit of measurement
☐	☒	An indication of whether measurements were taken from distinct samples or whether the same sample was measured repeatedly
☐	☒	The statistical test(s) used AND whether they are one- or two-sided *Only common tests should be described solely by name; describe more complex techniques in the Methods section.*
☒	☐	A description of all covariates tested
☐	☒	A description of any assumptions or corrections, such as tests of normality and adjustment for multiple comparisons
☐	☒	A full description of the statistics including central tendency (e.g. means) or other basic estimates (e.g. regression coefficient) AND variation (e.g. standard deviation) or associated estimates of uncertainty (e.g. confidence intervals)
☐	☒	For null hypothesis testing, the test statistic (e.g. *F*, *t*, *r*) with confidence intervals, effect sizes, degrees of freedom and *P* value noted *Give P values as exact values whenever suitable.*
☒	☐	For Bayesian analysis, information on the choice of priors and Markov chain Monte Carlo settings
☒	☐	For hierarchical and complex designs, identification of the appropriate level for tests and full reporting of outcomes
☒	☐	Estimates of effect sizes (e.g. Cohen's *d*, Pearson's *r*), indicating how they were calculated
☐	☒	Clearly defined error bars *State explicitly what error bars represent (e.g. SD, SE, CI)*

Our web collection on statistics for biologists may be useful.

Software and code

Policy information about availability of computer code

Data collection	*Provide a description of all commercial, open source and custom code used to collect the data in this study, specifying the version used OR state that no software was used.*
Data analysis	Peptide mass spectra were processed with an house SEQUEST-based software pipeline (Huttlin, E.L., et all. Cell. 143, 1174–1189 (2010). Details available upon reasonable request

For manuscripts utilizing custom algorithms or software that are central to the research but not yet described in published literature, software must be made available to editors/reviewers upon request. We strongly encourage code deposition in a community repository (e.g. GitHub). See the Nature Research guidelines for submitting code & software for further information.

Data

Policy information about availability of data

All manuscripts must include a data availability statement. This statement should provide the following information, where applicable:

- Accession codes, unique identifiers, or web links for publicly available datasets
- A list of figures that have associated raw data
- A description of any restrictions on data availability

Full scans for all western blots are provided in Supplementary Fig 1. Source Data for all mouse experiments have been provided. All other data are available from the corresponding author on reasonable request.

Field-specific reporting

Please select the best fit for your research. If you are not sure, read the appropriate sections before making your selection.

☒ Life sciences ☐ Behavioural & social sciences ☐ Ecological, evolutionary & environmental sciences

For a reference copy of the document with all sections, see nature.com/authors/policies/ReportingSummary-flat.pdf

Life sciences study design

All studies must disclose on these points even when the disclosure is negative.

Sample size	Sample sizes were determined on the basis of previous experiments using similar methodologies and are sufficient to account for any biological/technical variability.
Data exclusions	N/A
Replication	All experimental findings were reproduced as biological replicates at the value stated in figure legends, unless otherwise indicated. All additional replication attempts were successful.
Randomization	For in vivo studies, mice were randomly assigned to treatment groups. For MS analyses, samples were processed in random order and experimenters were blinded to experimental conditions.
Blinding	For MS analyses, samples were processed in random order and experimenters were blinded to experimental conditions.

Reporting for specific materials, systems and methods

Materials & experimental systems

n/a	Involved in the study
☒	☐ Unique biological materials
☐	☒ Antibodies
☐	☒ Eukaryotic cell lines
☒	☐ Palaeontology
☐	☒ Animals and other organisms
☒	☐ Human research participants

Methods

n/a	Involved in the study
☒	☐ ChIP-seq
☒	☐ Flow cytometry
☒	☐ MRI-based neuroimaging

Antibodies

Antibodies used	Antibodies used were pPKA substrate (CST 9624 s),Tubulin (Abcam AB44928) and anti-rabbit HRP (Promega).
Validation	CST statement: "To ensure product performance, we validate all of our antibodies, in-house, in multiple research applications."

Eukaryotic cell lines

Policy information about cell lines

Cell line source(s)	DE2.3 cells, C2C12, hepatocytes, osteocytes, lung A549 were from American Type Culture Collection (ATCC).
Authentication	No authentication was used
Mycoplasma contamination	They were not tested.
Commonly misidentified lines (See ICLAC register)	No commonly misidentified cell lines were used

Animals and other organisms

Policy information about studies involving animals; ARRIVE guidelines recommended for reporting animal research

Laboratory animals	Unless otherwise stated, mice used were male C57BL/6J (8–12 weeks of age; Jackson Laboratories), and housed in a temperature-controlled (23 °C) room on a 12 h light/dark cycle. Both male and female UCP1-KO (B6.129-Ucp1tm1Kz/J) and littermate matched heterozygotes were used. Brown adipocytes were cultured from male and female pups (2-6 days old).
Wild animals	N/A
Field-collected samples	N/A